Wayne State University Dissertations

1-1-2010

Raman Spectroscopic Modeling Of T- Lymphocyte Activation And Detection Of Acute Renal Allograft Rejection

Kristian L. Brown
Wayne State University,

Follow this and additional works at: http://digitalcommons.wayne.edu/oa_dissertations

Part of the Biomedical Engineering and Bioengineering Commons, Medical Biophysics Commons, and the Medical Immunology Commons

Recommended Citation

**RAMAN SPECTROSCOPIC MODELING OF T- LYMPHOCYTE ACTIVATION
AND DETECTION OF ACUTE RENAL ALLOGRAFT REJECTION**

by

KRISTIAN L. BROWN

DISSERTATION

Submitted to the Graduate School

of Wayne State University,

Detroit, Michigan

in partial fulfillment of the requirements

for the degree of

DOCTOR OF PHILOSOPHY

2010

MAJOR: BIOMEDICAL ENGINEERING

Approved by:

_____

Advisor: Date

_____

_____

DEDICATION

This dissertation and my overall doctoral body of work is dedicated to the two ladies in my life;

my wife and my daughter

ACKNOWLEDGEMENTS

Without the continued unconditional support and encouragement

that my family and the department of surgery have provided me, this accomplishment would

never have been possible. A very long time ago I decided that the goal of obtaining an MD and a

PhD was worth it. However, it has only been through witnessing the actual sacrifice made by my

family that I have arrived at a working understanding of its true value.

I also would like to thank the department of biomedical engineering and the entire college

of engineering for its embrace of a simple surgeon. My intellectual growth as a direct result of

working alongside brilliant engineers cannot be captured in words. There is something that can

be said about those who transform thoughts into palpable products through their genius.

TABLE OF CONTENTS

LIST OF TABLES

LIST OF FIGURES

CHAPTER 1- INTRODUCTION AND BRIEF HISTORICAL NOTE

The evolution of care concerning end-stage renal disease (ESRD) has been a multi-layered, multi-faceted one. Thomas Graham, the nineteenth century Scottish scientist who was best known for his pioneering work in the area of colloid chemistry, helped to establish principles of gas exchange (Graham's law) that were later incorporated into Willem Kolff's 1944 dialysis machine which was touted as the "first artificial kidney" [1, 2]. Despite the tremendous early success of hemodialysis, it would soon be supplanted as the preferred treatment for ESRD by a modality that had begun its quiet parallel development in Austria at the turn of the twentieth century. This modality was renal transplantation. Renal transplantation began in 1902 with the first successful animal-to-animal kidney transfer [3]. By 1909, the first human xenotransplantation had been conducted in France and despite the fact that it only functioned for one hour, it represented a huge clinical leap [4]. 1949 proved to be a milestone year in the growth of the fledgling discipline of renal transplantation, during which Sir Peter Medawar, a British zoologist, described acquired immune tolerance and the immunology of organ rejection for which he was later awarded the Nobel Prize [5, 6]. On the heels of this immunologic understanding, Joseph E. Murray performed the first truly successful kidney transplantation between identical twins in 1954 followed shortly by the first successful cadaveric kidney transplantation in 1962 performed by Samuel Kountz and Roy Cohn at Stanford University. For their contributions these men were held in high regard and like Medawar many years prior, Murray was awarded the Nobel Prize in 1990 for his contributions to transplantation medicine [7]. The next three decades would be embossed by advances in immunosuppressive therapy, with the inclusion of steroids (1963), azathioprine (1963), cyclosporine (1972), and mycophenolate mofetil (1995). This period would also mark the passage of the End Stage Renal

Disease Act (1972), which assured medical coverage for all patients with ESRD and would later be extended to cover transplantation expenses as well [8]. The benefits of the aforementioned advances would soon translate into improved patient survival. In 1973, an article published in the *Journal of the American Medical Association* reported on outcomes of 10,357 of the 12,389 transplants that were performed from 1951 to 1970. In this article, they noted that patient survival was 47.6% [9]. However, just 10 years later in 1983 the nationwide 1 year patient and graft survival had improved to 95% and 88%, respectively [10, 11]. With this new outcome data demonstrating the efficacy and potential promise of renal transplantation, it officially replaced hemodialysis as the preferred treatment for ESRD. Over the next decade (1990-2000), the growth of renal transplantation was substantial, increasing from approximately 7000 kidneys transplanted per year to 12,000 in the US. [12]. In addition, the emerging clinical innovations in immunosuppressive therapy, multidisciplinary treatment protocols, and surgical management helped to redefine the selection criteria for both renal allograft donors and recipients. Recipients who were once considered to be too high risk were now representing a sizable part of annual totals at many transplant centers [13, 14]. With more patients now being considered for renal transplantation, the disparity between the supply of available grafts and the demand has been exacerbated [15]. Organ Procurement and Transplantation Network data collected from January to August 2009 reported that there were 105,127 individuals on the waiting list for kidney transplants. For this same period, there were only 19,114 combined deceased- and live-donor grafts available [15]. In the face of this growing organ shortage, many efforts have been launched to mitigate this disparity. Some of these have included Organ Procurement Organization and United Network for Organ Sharing campaigns to educate the public about minimally invasive (laparoscopic) live-donor options as well as driver's license-based organ

donation programs [16, 17]. Despite these notable efforts, the organ supply simply has not kept pace with the demand. This is especially true when considering that the incidence of the major causes of ESRD (i.e. hypertension and diabetes) are on the rise [18, 19]. Based upon these observations, preservation of existing graft function and graft survival must be of paramount importance.

The research contained within this document is aimed at addressing acute rejection (AR) and the persistent threat that it poses to graft function and survival. It accomplishes this by presenting a foundational study regarding the development of a noninvasive method of detecting acute renal allograft rejection based upon the laser-based technological tool, Raman spectroscopy (RS).

The organizational structure of chapters 2 through 4 is designed to provide a working knowledge of transplant immunology and RS as well as familiarize the reader with a comprehensive review of the major non-Raman-based, noninvasive methodologies to detect AR that have been proposed to date. In addition, these chapters serve to outline the scope of the AR problem by highlighting the limitations of the current screening modality. Chapters 5 through 7 describe the experimental design, results, and conclusions for the various studies that were conducted to support our hypothesis that RS can effectively model T lymphocyte activation and serve as an eventual tool to noninvasively diagnose AR with high accuracy. Chapters 5 through 7 are each organized to present data that pertain to a particular investigational question. As a group, chapters 5 through 7 provide a three-pronged research approach to support the aforementioned hypothesis. This organizational theme allows improved flow of content and affords an intellectual structure for chapter 8 which comprehensively discusses the results of chapters 5 through 7 and draws all concepts contained herein to a global conclusion.

REFERENCES

1. Graham, T. Complete Dictionary of Scientific Biography. Charles Scribner's Sons. 2008. [cited 2009 24 Nov]. Available from: http://Encyclopedia.com.

2. Heiney P. 2003. The Nuts and Bolts of Life: Willem Kolff and the Invention of the Kidney Machine. Stroud: Sutton Publishing.

3. Tilney NL. 2003. Transplant: from myth to reality. New Haven, Conn. Yale University Press.

4. Hamilton D. 2001. Kidney transplantation: a history. In: Morris PJ, ed. Kidney transplantation: principles and practice. 5th ed. Philadelphia. W.B. Saunders. p. 1-8.

5. Sulek, K. 1969. Nobel Prize for F. M. Burnett and P. B. Medawar in 1960 for discovery of acquired immunological tolerance. Wiad. Lek. 22 (5): 505–506.

6. Robert A, Shampo M. 2003. Peter Medawar-discoverer of immunologic tolerance. Mayo Clin Proc 78 (4): 401, 403.

7. Murray J. 2001. Surgery of the Soul: Reflections on a Curious Career. Sagamore, MA. Science History Publications. Watson Publishing International.

8. Schneider M. 2006. Introduction to Public Health. 2nd ed. Toronto. Jones and Bartlett. p. 445-447.

9. Medicine Capsule [updated 2009 Oct 1]. Time Magazine. [cited 2009 November 12] http://www.time.com/time/magazine/article/0,9171,943512,00.html. Original article: December 24, 1973.

10. Rosenthal J, Hakala T, Iwatsuki S, Shaw B, Starzl T. 1983. Cadaveric Renal Transplantation Under Cyclosporine-Steroid Therapy. Surg Gynecol Obstet 157(4): 309–315.

11. Belzer F, Corry R, Diethelm A, Mendez R, Salvatierra O, Tilney N, Cerilli J. 1981. Current Results and Expectations of Renal Transplantation. JAMA 246(12):1330-1331.

12. Spring 2007 Regional Meeting Data of the U.S. Organ Procurement and Transplantation Network and the Scientific Registry of Transplant Recipients. [updated May 2007] . OPTN. [cited 2009 November 12] http://www.optn.org/latestData.

13. Brown KL, El-Amm JM, Doshi MD, Singh A, Morawski K, Cincotta E, Siddiqui F, Losanoff JE, West MS, Gruber SA. 2008. Intermediate-term outcomes of hepatitis C-positive compared with hepatitis C-negative deceased-donor renal allograft recipients. Am J Surg 195(3):298-302; discussion 302-303.

14. Gruber SA, Doshi MD, Cincotta E, Brown KL, Singh A, Morawski K, Alangaden G, Chandrasekar P, Losanoff JE, West MS, El-Amm JM. 2008. Preliminary experience with renal transplantation in HIV+ recipients: low acute rejection and infection rates. Transplantation 86(2):269-274.

15. Compiled Data from the U.S. Organ Procurement and Transplantation Network and the Scientific Registry of Transplant Recipients. 2009 [updated June 2009]. OPTN [cited 2009 November 12] http://www.optn.org/latestData.

16. National Kidney Foundation. Drive to increase living donor participation. [updated 2009 Feb]. http://www.kidney.org/transplantation/livingDonors/infoLinks.cfm.

17. Social and Behavioral Interventions to Increase Solid Organ Donation Grantees – Fiscal Years 1999-2009. [cited 2009 November 12]. http://organdonor.gov/research/index.htm.

18. Hajjar I, Kotchen J, Kotchen T. 2006. Hypertension: trends in prevalence, incidence, and control. Annu Rev Public Health 27:465-490.

19. Kramer H, Cao G, Dugas L, Luke A, Cooper R, Durazo-Arvizu R. 2009. Increasing BMI and waist circumference and prevalence of obesity among adults with Type 2 diabetes: the National Health and Nutrition Examination Surveys. J Diabetes Complications In Press. DOI: 10.1016/j.jdiacomp.2009.10.001.

CHAPTER 2- CLINICAL AND IMMUNOLOGICAL BACKGROUND

2.1- Immunologic Overview

In order to gain a better understanding of the mechanisms driving organ rejection and how RS can be used in its detection, a brief review of the immune system is in order. The immune system is comprised of several cellular and non-cellular components and is organized with respect to function in response to a foreign antigen or pathogen. It can be divided into the innate and adaptive immune systems [1].

The innate immune system is the initial responder to foreign antigens. The role of this system is to contain, mitigate, and if possible, eliminate the pathogen/antigen within the first 2-3 days following infection/pathogen introduction [1]. The innate immune system can be subdivided into barrier, neutralization, and elimination components. The barrier components consist of the skin and mucous, which are crucial to maintaining an effective partition to the external environment. The neutralization and elimination of foreign antigens is carried out by polymorphonuclear cells (PMN; also known as neutrophils), natural killer cells (NKC), dendritic cells, macrophages, eosinophils, mast cells, and to a lesser extent, basophils. In addition, innate immunity utilizes the complement system. This system of factors and enzymes is involved in coating the surface of pathogens thus making them more susceptible to phagocytosis, cell lysis, and elimination [1].

The adaptive immune response is tailored according to the particular type of pathogen that is present. Unlike the innate immune system which is initiated immediately, the adaptive immune system requires 5-10 days to mount a full response to a *primary* infection or introduction to foreign antigen. This response is carried out through the actions of B and T

lymphocytes. A summary of how the two aforementioned divisions of the immune system are

organized is depicted in **figure 1.**
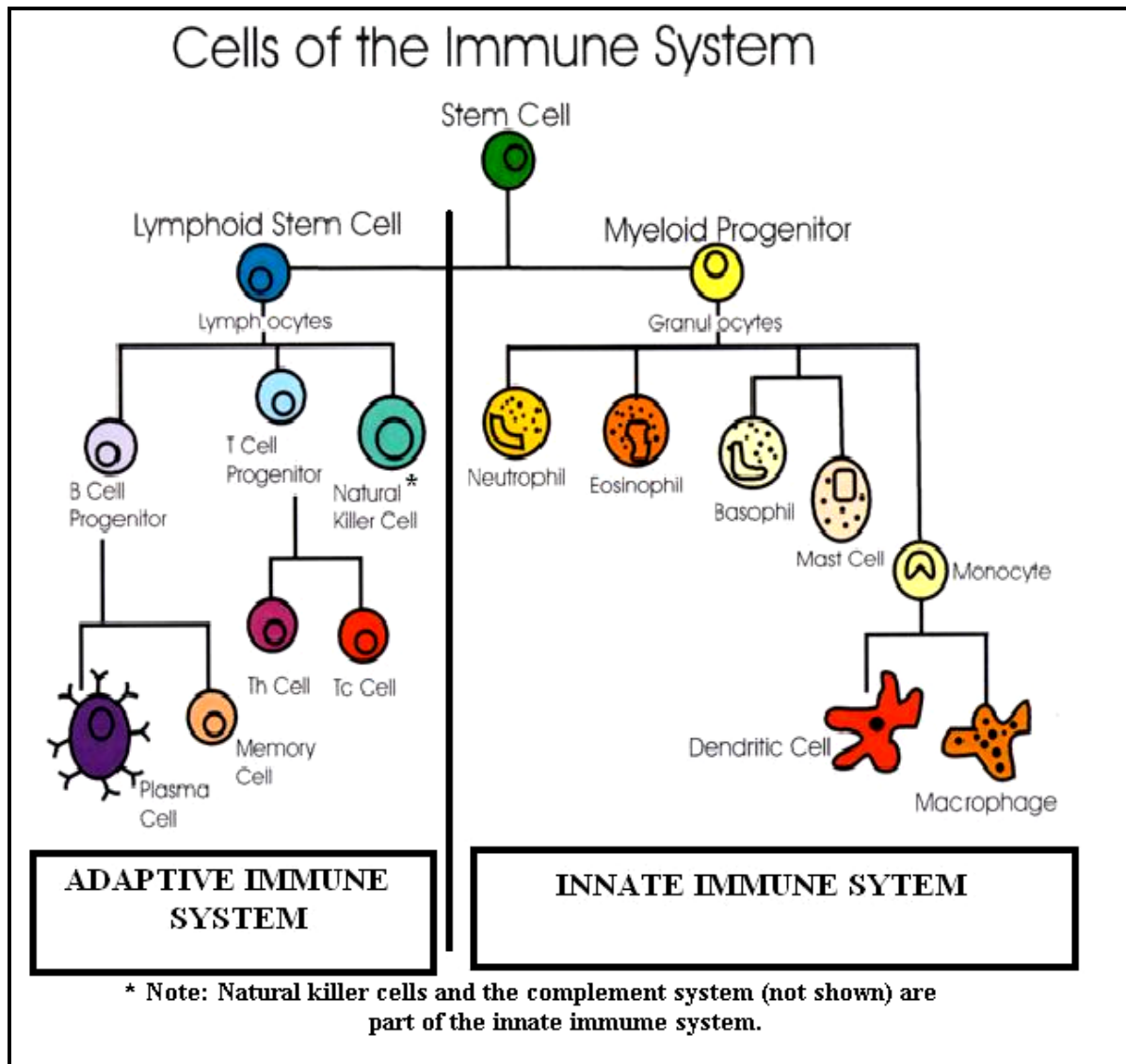
Figure 1. Organizational scheme of the adaptive and innate cells of the immune system [1].

B lymphocytes are primed and activated by T lymphocytes. These activated forms of B lymphocytes are called plasma cells which are capable of producing and releasing antibodies or immunoglobulins (Igs). There are five classes of Igs; IgG, IgA, IgM, IgD, and IgE [1]. These Igs possess a conserved Fc region and a variable Fab domain. This variable Fab domain allows each Ig to take on over 10^{14} different structural forms [2]. These Igs aid in the neutralization process by coating and tagging the foreign antigen for elimination. Igs can also act directly on infected cells using a complement directed membrane attack complex that results in holes being placed in the membrane leading to cell lysis [2].

The T lymphocyte makes up about 80% of the total circulating lymphocytes [1]. Structurally, the T cell receptor (TCR) has a similar structure to the Fab portion of the Ig [2]. The heterodimeric receptor has both an alpha (α) and beta (β) subunit which is composed of N-terminal Ig variable domain, one Ig-constant domain, a transmembrane/cell membrane-spanning region, and a short cytoplasmic tail at the C-terminal end [3]. The N-terminal variable domains of both the TCR α-chain and β-chain have three complementarity determining regions (CDRs), CDR1, CDR2, and CDR3. These CDRs are hyper-variable regions which allow myriads of possible antigen binding combinations. There is an additional variable region of the β-chain (HV4) which also has a hyper-variability region. However, this HV4 region does not normally contact major histocompatibility complex (MHC)-bound peptide antigens but is essential in the binding of non-specific and superantigens (i.e. CD3/CD28-coated activation beads and mitogens, respectively) [3]. These residues are situated at the interface of the α- and β-chains and in the β-chain framework which is thought to be involved in binding the CD3 complex. The CDR that is responsible for the majority of antigen recognition is the CDR3. CDR1 of the α chain interacts with the N- terminus of the antigen peptide whereas the CDR1 of the β chain is involved in

binding the C- terminus of the antigen peptide. CDR2 is thought to recognize the MHC [3].

T lymphocytes express either CD4 or CD8. These cell surface molecular subtypes are derived from a differentiation process that occurs in the thymus early in immunologic development. This process designates CD4+ cells as T helper lymphocytes and CD8+ cells as cytotoxic T lymphocytes. T lymphocytes work intimately with antigen presenting cells (APCs) of the innate immune system, which are specialized cells capable of phagocytosis of foreign antigens. These antigens are processed and presented to the T lymphocyte via the highly conserved cell surface molecule, the MHC. There are two classes of MHC molecules, designated I and II. Class I MHCs are found on all nucleated cells, whereas only cells that possess phagocytotic properties (i.e. dendritic cells, macrophages, PMNs, B lymphocytes) co-express MHC class II molecules. MHC class I and II molecule interact with the TCR of CD4+ and CD8+, respectively. This interaction is termed signal 1. Signal 1 leads to T lymphocyte activation and clonal expansion only in the presence of the co-stimulatory feedback, signal 2. This involves the T cell's CD28 binding to the APC's CD80. In the absence of signal 2 the T lymphocyte undergoes anergy and is prevented from activating (**Figure 2**) [4].
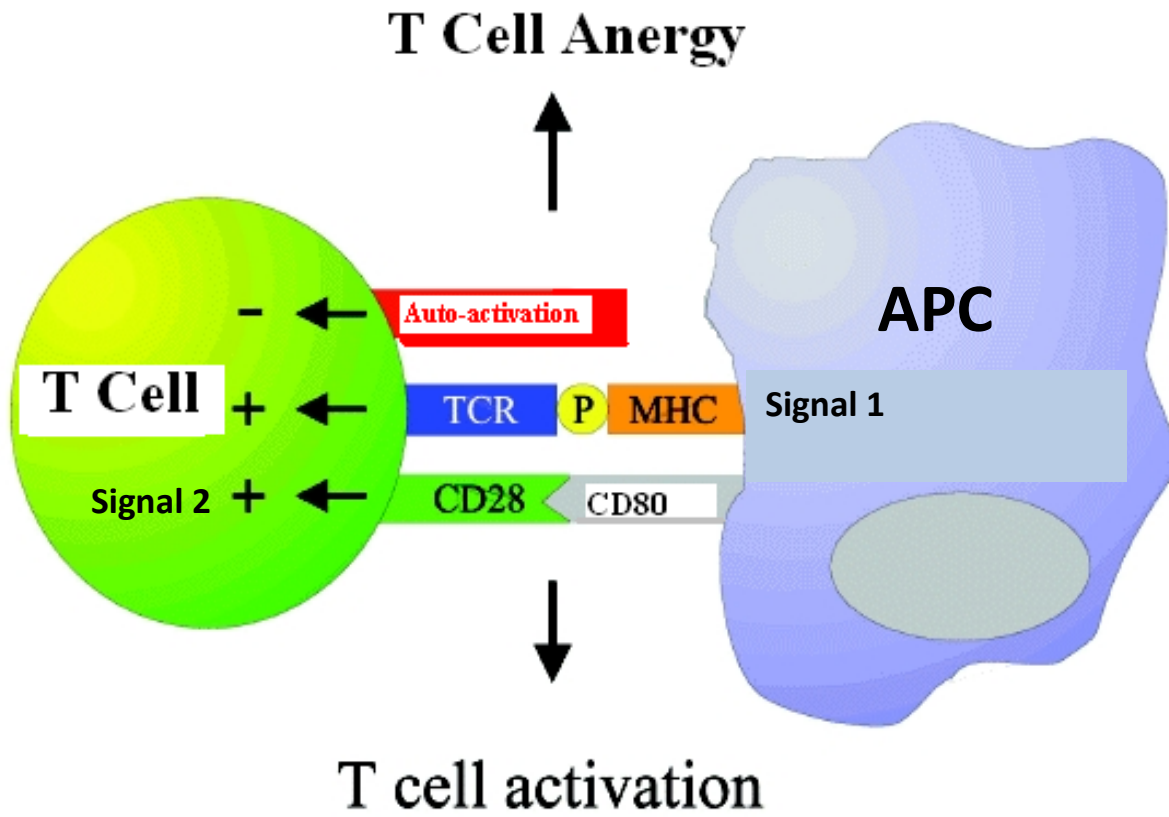
Figure 2. The binding of TCR- MHC complex (signal 1) and CD28-CD80 complex (signal 2) leading to T cell

activation or in the absence of signal 2, anergy [4].

In the presence of a proper signal 1 and 2 the T lymphocyte is activated. For this research investigation, T lymphocyte activation was defined as *an increase in immune-specific DNA transcription/translation, dimerization of CD3 with the TCR, and the characteristic up-regulation of cell surface receptors, notably CD69, CD25, and CD71* [1, 5-7].

The mechanisms of these activation events begin with the binding of a ligand (MHC) to the TCR which is followed by CD3, CD4, and TCR clustering. This is facilitated by phosphorylation of tyrosine residues on the cytosolic face of the plasma membrane [8]. This initial tyrosine kinase-driven step is common to all forms of activation regardless of the particular ligand or stimulus. Initial receptor clustering is followed by phosphorylation of zeta chain-associated protein kinase 70 (Zap-70) which in turn phosphorylates phospholipase C- γ (PLC). PLC leads to three important activation pathways. The first involves the activation of guanine-nucleotide exchange factor which results in the activation of mitogen activated protein (MAP) kinase and ultimately the activator protein-1 (AP-1) transcription factor. The second pathway activated by PLC leads to the cleavage of phosphatidylinositol bisphosphate (PIP_2) to yield diacylglycerol (DAG). DAG and Ca^{2+} activate protein kinase C culminating in the activation of the transcription factor, NF kappa B. The third pathway begins with PLC cleaving PIP_2 into inositol triphoshate (IP_3). IP_3 increases cytosolic calcium levels activating calcineurin which works directly to increase the activity of nuclear factor of activated T cells (NFAT). The main transcription factors from all three pathways (AP-1, NF kappa B, and NFAT) lead to an increase in immune-related gene transcription, cell proliferation, and differentiation [8]. **Figure 3** summarizes these activation events.
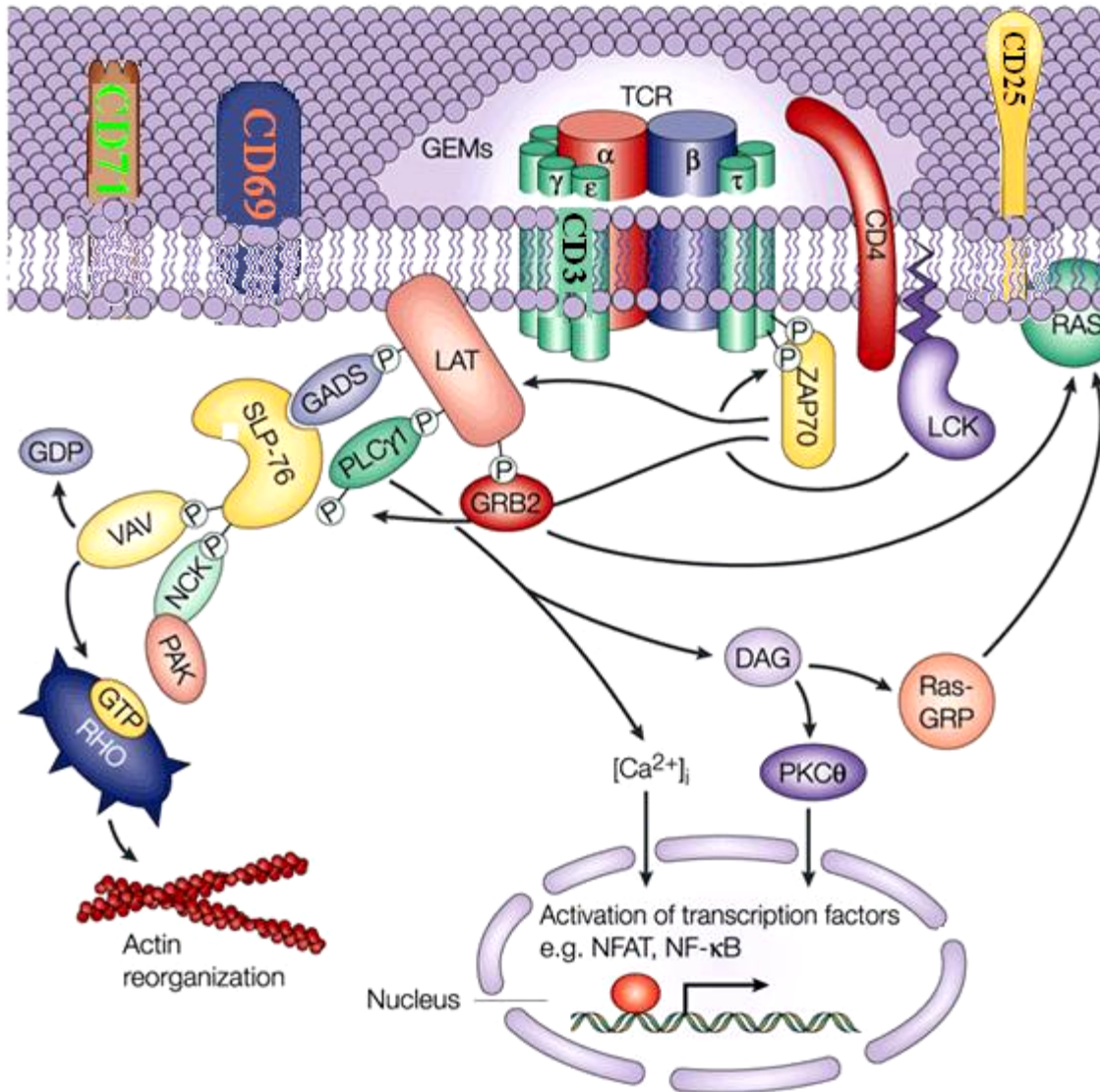
Figure 3. T lymphocyte intracellular activation pathway [9].

A key step in the aforementioned early activation process is the clustering and subsequent binding of CD3 with the TCR (**Figure 4**). CD3 is present at low levels on the surface of non-activated T lymphocytes [1]. The binding of the MHC to the TCR triggers intracellular activation of LcK and Zap-70 which phosphorylates the cytoplasmic tails of CD3 resulting in assembly of its subunits. This CD3 complex then binds the TCR leading to a conformational change in the 3 dimensional (3D) structure of the TCR-MHC union (**Figure 5**). It is important to note that even when the MHC is released from the TCR-CD3 complex, the TCR-CD3 complex remains at a different conformational state and 3D structure than the un-stimulated TCR and non-clustered CD3 subunits [10,11].
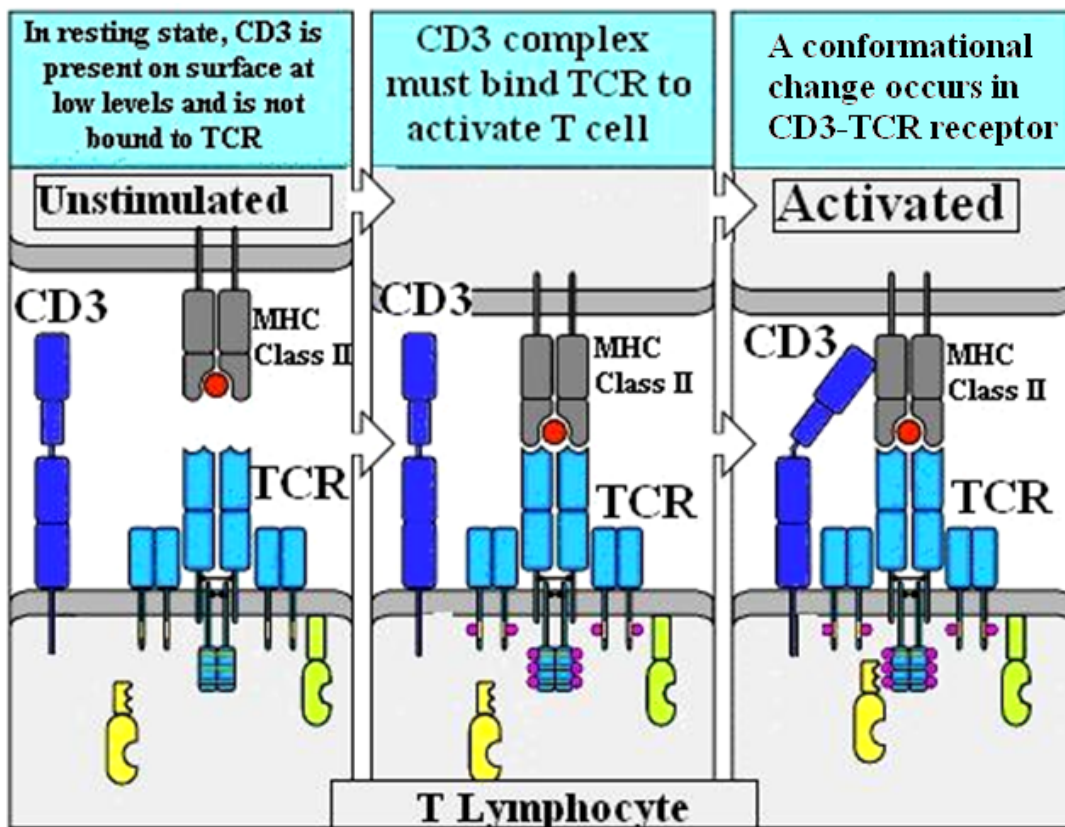
Figure 4. Dimerization of CD3 complex and TCR is necessary for T lymphocyte activation [10].
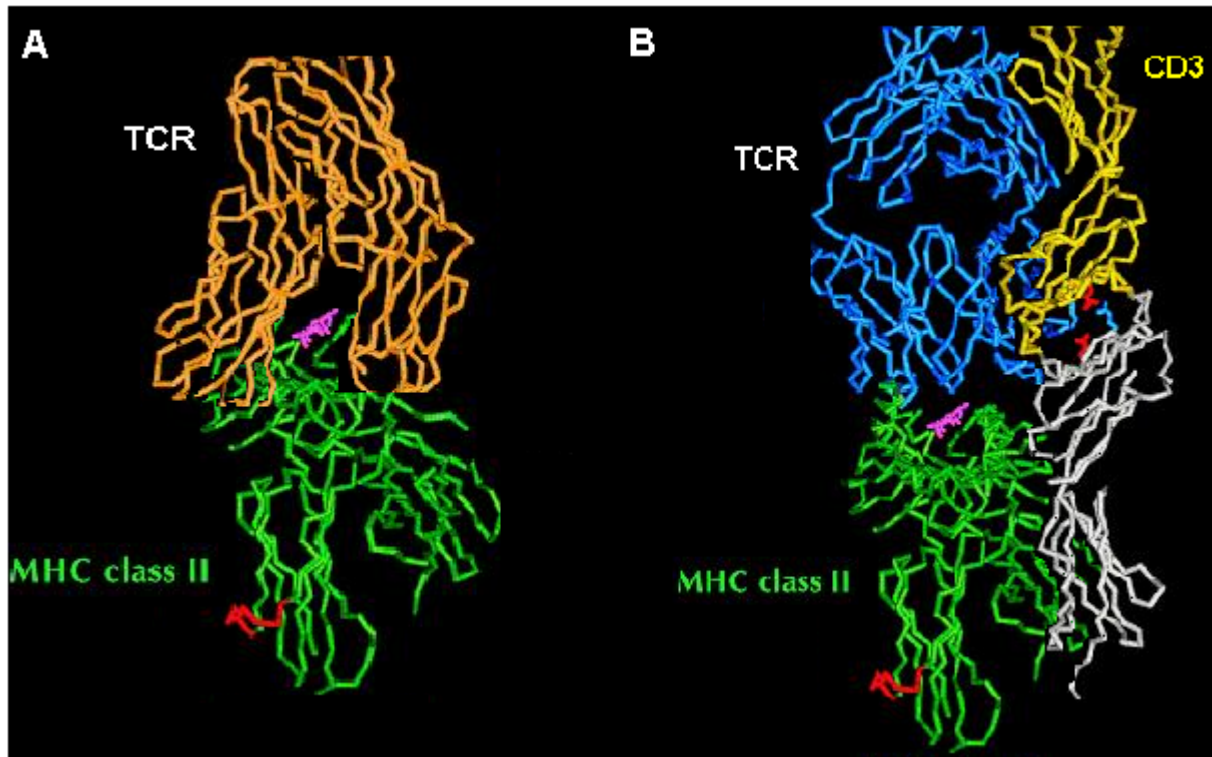
Figure 5. Conformational change in the TCR-MHC union before (A) and after (B) CD3 binding. There is significant alteration in 3D structure of the TCR noted in the superior aspect of the diagram. Antigen peptide shown in pink; anchor protein (MHC II) and stabilizing protein (CD3) are shown in red [11].

This conformational change is not only essential to the initiation of the intracellular activation cascade, but also significantly alters the exposed molecular residues on the T cell surface transforming the topographic profile involved in light scattering. These surface changes are amplified by the addition of the up-regulated CD25, CD69, and CD71 receptors. In fact, there are over 10^{18} structurally different receptors on the surface of activated T lymphocytes, as compared to its non-activated counterparts [12]. It is this specialized up-regulation of cell surface

receptors and subsequent change in molecular topography that provides the key to identifying activated T lymphocytes using RS.

2.2- The Immunologic Basis of Renal Allograft Rejection

Allograft rejection can be divided into three main categories; hyperacute, acute, and chronic rejection. This classification is based on the timing and nature of histopathologic changes in the transplanted organ as well as the particular biologic component of the immune system that drives the process. It is important to note that these rejection processes are not discretely separate events. Instead, they exist on a continuum of immunologic response to foreign allograft antigens.

Hyperacute rejection is caused by preformed antibodies in the recipient directed toward the endothelium of the donor graft [13]. These antibodies bind to the vascular endothelium activating the complement and clotting cascades which result in obstruction of graft vessels, parenchymal congestion, and death of the graft within minutes (**Figure 6**) [13]. Fortunately, this irreversible process is rare due to the routine use of prospective cytotoxic crossmatching which screens for the preformed antibodies [14].
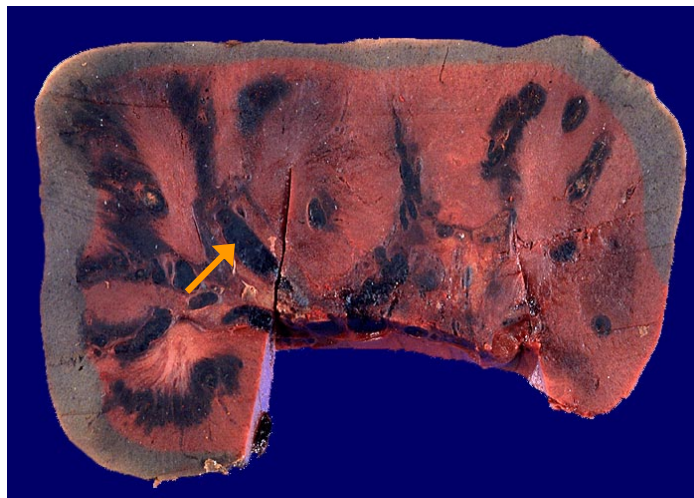
Figure 6. Gross specimen of kidney illustrating hyperacute rejection with focal areas of infarction (arrow) [12].

Chronic rejection remains a poorly understood inflammatory process that has many immunologic and non-immunologic causes including, but not limited to, ischemic-reperfusion injury, cytomegalovirus (CMV) infection, multiple episodes of AR, and calcineurin inhibitor/sirolimus toxicity [15]. The pathohistologic findings can be characterized by concentric atherosclerosis of vessels coupled with glomerulo-tubular fibrosis and atrophy [16, 17]. The predominant cell found within graft vessels and tissues late in chronic rejection is the macrophage [1]. These cells are attracted by chemokines that cause the maturation of monocytes (the immature blood-dwelling form of macrophages) and their infiltration into tissues via endothelial adhesion molecules. Once in the tissues, macrophages secrete high levels of IL-1 and TNF-α which lead to further macrophage recruitment [1]. The result of this inflammatory activity is progressive nephron fibrosis often termed chronic allograft nephropathy (CAN) [17].

The activated T lymphocyte is both necessary and sufficient to induce AR [1]. Whether it is the recognition of non-self via foreign MHC class I molecules in the periphery by CD8+ cytotoxic T cells or the interrogation of graft-derived foreign APCs in host lymph nodes by CD4+ helper T cells, the activated T lymphocyte is central to the initiation of a immunological cascade culminating in renal allograft destruction in the acute setting [1]. The histopathologic findings of AR range from foci of moderate tubulitis to severe intimal arteritis with focal infarction, depending on the severity or grade. The particular grades of AR are described by the Banff 97 criteria and are illustrated in **Appendix A** [18].

2.3- Clinical Implications of Allograft Rejection

AR can cause graft dysfunction and on occasions, complete graft loss [19, 20]. AR most commonly occurs within the first 6 months following transplantation. The incidence of AR ranges from 3% to 22% and is dependent upon the individual transplant center, source of graft

(deceased vs. live donor), panel reactive antibody levels, and recipient risk factors [21, 22]. Moreover, it has been well documented that African Americans, pediatric, and retransplant patients have a higher incidence of AR when compared with their Caucasian, adult, primary transplant counterparts [22]. The negative clinical impact of AR on graft outcomes has also been well described. In a study looking at deceased-donor renal allografts transplanted over a 7 year period, it was reported that the half-life of the graft increased from 7.0 to 17.9 years in the absence of current or previously reported AR episodes. On the other hand, grafts that had one or more reported episodes showed only a marginal increase in half-life from 7.0 to 8.8 years over the same time period [23]. This data suggests that although AR is reversible in most cases, its occurrence, severity, and timing negatively affect graft survival. Clearly, the earlier that adjustments to the immunosuppressive regiment aimed at reversing the episode can be made, the better the subsequent functional result. However, this early diagnosis is difficult with current modalities. Reliable screening for AR has proven problematic due its deceptively benign presentation as an asymptomatic elevation in serum creatinine. This abnormal increase in serum creatinine of 25% or greater compared with a post-transplant baseline is used by most centers as a marker for AR [24]. Despite its routine usage, serum creatinine elevation is a late finding which manifests only after rejection has been present long enough to cause significant histologic damage to nephrons leading to disruption in renal function and a subsequent decrease in clearance. In addition to being a late finding of AR, elevations in serum creatinine have a low sensitivity, since subclinical AR (SCAR) can occur with no detectable change in serum creatinine [25]. SCAR has prompted a greater implementation of protocol renal transplant biopsies in response to concerns over the accelerated development of CAN if the condition remains undetected and untreated [26, 27]. Moreover, serum creatinine lacks specificity as a

marker, largely due to the observation that urinary tract infections, abnormal blood glucose levels, and dehydration can cause false positives [28]. Even immunosuppressive medications, mainly tacrolimus and cyclosporine, can lead to nephrotoxicity which clinically presents as elevations in serum creatinine [14]. This late, non-sensitive, non-specific modality of detecting AR has also prompted many patients to undergo unnecessary biopsies. These biopsies come with the risks of pain, bleeding, infection, creation of artereriovenous fistulae, and in rare cases loss of graft [29, 30]. Coupled with the risks posed to patients, biopsies are subject to sampling errors and represent a significant financial burden on the health care system [31]. Based upon the limitations of the current screening modality for AR, a rapid, noninvasive screening tool that provides both a high sensitivity and specificity is highly desirable.

REFERENCES

1. Janeway C, Travers P, Walport M, Capra J. 1999. Immunobiology: The immune system in health and disease. 4th edition. Garland Publishing, NY. p. 294-298.

2. Litman G, Rast J, Shamblott M (1993). "Phylogenetic diversification of immunoglobulin genes and the antibody repertoire". *Mol. Biol. Evol.* **10** (1): 60–72

3. Kieke M, Shusta E, Teyton L, Wittrup D, Kranz D. "Selection of functional T cell receptor mutants from a yeast surface-display library", *Proceedings of the National Academy of Science of the United States of America* **96** (10): 5651–5656

4. Adapted from: Olsson M, Hagnerud S, Hedelius D, Oldenborg P . Hematologic Diseases: Autoimmune Hemolytic Anemia and Immune Thrombocytopenic Purpura. http://www.ncbi.nlm.nih.gov/bookshelf/br.fcgi?book=eurekah&part=A36437.

5. Bernard A, Boumsell L, Hill C. 1984. Joint report of the first international workshop on human leucocyte differentiation antigens by the investigators of the participating laboratories. In: Bernard A, Boumsell L, Dausset J, Milstein C, Schlossman SF, eds. Leucocyte Typing. New York, NY: Springer-Verlag. 9-108.

6. Chen J, Prince H, Buck D, et al. 1988. Leu-23: an early activation antigen on human lymphocytes. Fed Proc 2:A1214.

7. Testi R, Philips J, Lanier L. 1989. Leu-23 induction as an early marker for functional CD3/T cell antigen receptor triggering: requirement for receptor cross-linking, prolonged elevation of intracellular (Ca^{++}), and stimulation of protein kinase C. J Immunol 142:1854.

8. Signaling through immune system receptors. Immunobiology. NCBI Bookshelf. http://www.ncbi.nlm.nih.gov/bookshelf/br.fcgi?book=imm&part=A673. 1/2/2010.

9. Adapted from: Robert T. Abraham & Arthur Weiss. Jurkat T cells and development of the T-cell receptor signaling paradigm. Nature Reviews Immunology 4, 301-308 (April 2004) and Linsley PS, Ledbetter JA. The role of the CD28 receptor during T cell responses to antigen. *Annu Rev Immunol.* 1993; 11: 191–212.

10. Kjer-Nielsen L, Dunstone M, Kostenko L, Ely L, Beddoe T, Mifsud N, et al. 2004. Crystal structure of the human T cell receptor CD3εγ heterodimer complexed to the therapeutic mAb OKT3. PNAS 101(20). P 7675-7680.

11. Adapted from: Kaas and Lefranc, In Silico Biol. 5, 0046 (2005).

12. http://uhaweb.hartford.edu/BUGL/immune.htm#adapt (2002)

13. Higgins RM, Bevan DJ, Carey BS, Lea CK, Fallon M, Bühler R, Vaughan RW, O'Donnell PJ, Snowden SA, Bewick M, Hendry BM. 1996. Prevention of hyperacute rejection by removal of antibodies to HLA immediately before renal transplantation. Lancet 348(9036):1208-1211.

14. Janeway C. Travers P. Walport M. Capra J. 1999. T Cell Mediated Immunity. In: Austin, P., Lawrence, E. Immunobiology: The immune system in health and disease 4th edition. Garland Publishing, NY. p. 515-519.

15. Paramesh A, Grosskreutz F, Sander S, GondolesiG. Sharma, et. al. 2004. Thrombotic microangiopathy associated with combined sirolimus and tacrolimus

immunosuppression after intestinal transplantation. Transplantation 77(1): p. 129-131.

16. Nankivell B, Borrows R, Fung C, O'Connell P, Allen R, Chapman J. 2003. The Natural History of Chronic Allograft Nephropathy. NEJM 349:2326-2333.

17. Freese P, Svalander C, Mölne J, Nordén G, Nyberg G. 2001. Chronic allograft nephropathy- biopsy findings and outcome. Nephrol Dial Transplant 16: 2401-2406.

18. Bogman M and Dooper M. 1995. Banff classification for the histologic diagnosis of renal graft rejection: what are the advantages? Nephrol Dial Transplant: Editorial comments: p. 1291-1293.

19. Cosio FG, Pelletier RP, Falkenhain ME, Elkhammas EA, Davies EA, Bumgardner GL, Ferguson RM. 1997. Impact of acute rejection and early allograft function on renal allograft survival. Transplantation 63: 1611.

20. Tesi RJ, Henry ML, Elkhammas EA, Ferguson RM. 1993. Predictors of long-term primary cadaveric renal transplant survival. Clin Transplant 7: 345.

21. Meier-Kriesche HU, Ojo A, Magee J, Cibrik D, Hanson J, Leichtman A, and Kaplan Bruce. 2000. African-American renal transplant experience decreased risk of death due to infection: possible implications for immunosuppressive strategies. Transplantation 70 (2). p. 375-379.

22. Hardinger K, Stratta R, Egidi F, et al. 2001. Renal allograft outcomes in African American versus Caucasian transplant recipients in the tacrolimus era. Surgery 130. (4).

23. Hariharan S, Johnson CP, Bresnahan BA, Taranto SE, McIntosh MJ, Stablein D. 2000. Improved graft survival after renal transplantation in the United States, 1988 to 1996. N Engl J Med 342:605.

24. Gaber LW, Moore LW, Alloway RR, Flax SD, Shokouh-Amiri MH, Schroder T, Gaber AO. 1996. Correlation between Banff classification, acute renal rejection scores and reversal of rejection. Kidney Int 49 (2): p. 481-487.

25. Nankivell BJ, Borrows RJ, Fung CLS, O'Connell PJ, Allen RD, Chapman JR. 2004. Natural history, risk factors and impact of subclinical rejection in kidney transplantation. Transplantation 78: p. 242-249.

26. Nankivell BJ, Fenton-Lee CA, Kuypers DR, Cheung E, Allen RD, O'Connell PJ, Chapman JR. 2001. Effect of histological damage on long term kidney transplant outcome. Transplantation 71: p. 515-523.

27. Nankivell BJ, Borrows RJ, Fung CLS, O'Connell PJ, Allen RD, Chapman JR. 2003. The natural history of chronic allograft nephropathy. N Eng J Med 349: p. 2326-2333.

28. A J Matas, R L Simmons, C M Kjellstrand, and J S Najarian. 1977. Pseudorejection: factors mimicking rejection in renal allograft recipients. Ann Surg. 186(1): p. 51–59.

29. Mackie GC, Davies PF, Challis DR, Middleton IS. 2004. Renal infarction secondary to a subcapsular haematoma following percutaneous renal biopsy. Australas Radiol. 48(2): p. 207-210.

30. Machida J, Kitani K, Inadome A, Wada Y, Kawabata K, Yoshida M, Ueda S. 1996. Subcapsular hematoma and hypertension following percutaneous needle biopsy of a transplanted kidney. Int J Urol 3(3): p. 228-230.

31. Ellingsen A, Nyengaard J, Osterby R, Jurgensen K, Peterson S, Marcussen N. 2002. Measurements of cortical interstitium in biopsies from human kidney grafts: how representative and how reproducible? Nephrology Dialysis Transplantation 17: p. 788-792.

CHAPTER 3- REVIEW OF PROPOSED NONINVASIVE METHODS FOR DETECTING ACUTE REJECTION

In response to the aforementioned fundamental problems with using serum creatinine as a marker for AR, many proposed biomedical technologies to detect AR have been explored. Some require disruption of cellular biology and immunological integrity while others that are successful in studying the immune system in its confluent form are limited by the need to analyze byproducts of an up-regulated immune system. These byproducts are often subject to influence by both endogenous and exogenous factors which makes direct correlation with the presence of AR difficult. Li and colleagues [1] have proposed using polymerase chain reaction (PCR)-based methodologies in the measurement of urinary mRNA specific for granzyme B and perforin, two proteins that are increased in the inflammation/infection process. Limitations of this proposed AR screening modality are based on the observation that these mRNAs are non-specific and may be up-regulated in cases of inflammation, infection, as well as T cell mediated allograft rejection, and thus fail to address the issue of specificity. In addition, PCR technology, though a more prevalent part of clinical laboratory tests, still requires significant expertise and labor, making it a less than desirable screening tool. Sarwal and colleagues [2] have proposed using biopsy samples to identify characteristic gene expressions which are associated with clinical AR. Though a promising concept, this Genechip© technology still relies on obtaining invasive biopsy samples which are not without risk and are still subject to sampling error. Moreover, the patient selection process (who is chosen for biopsy) is dependent on less than accurate selection criteria (serum creatinine) thus leaving the issues of unwarranted referral and burden to the health care system unresolved. Even when considering Hildalgo and colleagues [3] proposed use of RNA microarrays that are carried out from peripheral blood-derived T lymphocytes, the infrastructure, costs, and labor intensive processing once again disqualify it as a

practical screening tool. Wishart and colleagues [4] have suggested using metabolomics as an AR detection modality. This mass spectrometry-based technology focuses on identifying increased levels of key metabolites that are produced in the setting of AR, mainly trimethylamine-N-oxide (TMAO) and dimethylamine (DMA). Although it adequately addresses the specificity question, there are still two major limitations to this screening modality. First, the clearance of the aforementioned metabolites can be strongly influenced by medications such as, cyclosporine or tacrolimus that may compete at the level of hepatic transporters (i.e. cytochrome P450) [5]. This is of concern in the transplant patient population due to the many comorbidities that require medicinal management. Secondly, many of these patients have impaired liver function due to previous alcohol use, and/or hepatitis disease, which may alter liver metabolism and elimination kinetics and drastically affect the sensitivity and specificity of this method. Finally, the analysis of Metabolomics-derived data requires software which utilizes intricate numerical methods thus increasing cost and requiring specialized knowledge and/or training [4].

One possible solution to the many limitations of the noninvasive methodologies stated above is to *directly* study the principal immune effector cell, the T lymphocyte, in the confluence of its actions within the intact immunological landscape in a noninvasive manner with a system that does not require labor-intensive preparation, processing, or analysis. Such a methodology would thereby avoid byproducts, invasive biopsies, varying patient pharmacokinetics, unjustifiable costs, and delays in diagnosis. We propose that RS represents such a methodology.

REFERENCES

1. Li B, Hartono C, Ding RD, Sharma VK, Ramaswamy R, Qian B, Serur D, Mouradian J, Schwartz JE, Suthanthiran M. 2001. Noninvasive diagnosis of renal-allograft rejection by measurement of messenger RNA for perforin and granzyme B in urine. N Engl J Med 344: p. 947–954.

2. Sarwal M, Chua MS, Kambham N, Hsieh SC, Satterwhite T, Masek M, Salvatierra O Jr. 2003. Molecular heterogeneity in acute renal allograft rejection identified by DNA microarray profiling. N Engl J Med 349(2): p. 125-38.

3. Hildalgo L, Einecke G, Allanach K, Halloran P. 2008. The transcriptome of human cytotoxic T cells: Similarities and disparities among allostimulated CD4+ CTL, CD8+ CTL and NK cells. American Journal of Transplantation 8: 627-636.

4. D. S. Wishart. 2005. Metabolomics: The principles and potential applications to transplantation. American Journal of Transplantation 5 (12), p. 2814–2820.

5. Gruber SA, Doshi MD, Cincotta E, Brown KL, Singh A, Morawski K, Alangaden G, Chandrasekar P, Losanoff JE, West MS, El-Amm JM. 2008. Preliminary experience with renal transplantation in HIV+ recipients: low acute rejection and infection rates. Transplantation 86(2). p. 269-74.

CHAPTER 4- RAMAN SPECTROSCOPY AS A DIAGNOSTIC TOOL

Chapter 4.1- Historical Background of Raman Spectroscopic Technology

The original concept of quantitative scattered light was proposed by the Austrian theoretical physicist, Adolf Smekal (1895-1959) in 1923 [1]. However, the phenomenon was not actually observed until 1928 when young Indian physicist Chandrasekhara Venkata Raman (1888-1970) along with K S Krishnan (1898-1961) demonstrated that light reflected back from an object was not merely light reflecting back unchanged (i.e. elastic fraction of scattered light) [2]. Instead, there was also a fraction of scattered light that reflected back with a different wavelength (i.e. inelastic fraction of scattered light). By utilizing sunlight passed through a narrow-band photographic filter to create monochromatic light and a crossed filter to differentially subtract out this monochromatic light, Raman was able to recreate and observe what was only theorized by Smekal [2]. In 1930, Sir Raman was awarded the Nobel Prize in physics for his contributions to the technologic tool that now bears his name. His original experimental design would be further refined through the years by Placzek, Bethe, Teller, Frisch, and many other prominent physicists [3].

Modern-day RS has proved invaluable in the fields of material science and chemical engineering due to its ability to characterize substances based upon their vibrational, rotational and other low energy modes [4]. The scattered fraction of light is generated when light interacting with the molecule being studied polarizes electrons surrounding the nuclei. This polarization reflects a transient or virtual state of the photon. When this interaction leads to electron distortion alone, the resultant frequency change is small and the scattered light is of the elastic type often referred to as Rayleigh scattering [5]. As depicted in **Figure 7**, this light returns

to the source unchanged. However, if nuclear motion occurs as a result of the light interacting with the molecule, then measurable energy will be transferred between incident photon and molecule generating an inelastic fraction of scattered light called Raman scattering [5]. Raman scattering can be further divided into stokes and anti-stokes scatterings (**Figure 7**). When the final ground state of the molecule has more energy than the initial state, the photon emitted will be at a lower frequency. This is known as Stokes Raman scattering. However, when the final state has less energy than the initial state, the emitted photon will have higher frequency than the excitation frequency and is considered anti-Stokes Raman scattering (**Figure 7**) [5]. The aforementioned scattering process can be represented by the following expressions [2]:

$$hv_s = hv_o \pm hv_m.$$ (1)

Here, h is the Planck's constant, v represents frequency, hv_o is the incident photon energy, hv_s is the scattered photon energy, and hv_m is the difference between the lowest and the first excited energy levels. In studies involving RS, Raman shift is usually the metric which is given by the equation:

$$\Delta v = v_0 - v_s$$ (2)

However, this is most often expressed in wavenumber (cm^{-1}):

$$v = c / \lambda$$ (3)

Here c represents the speed of light. Combining expressions 1-3 yields the Raman shift given as:

$$\Delta \bar{v} = v_0 \pm v_s = c \left(\frac{1}{\lambda_o} - \frac{1}{\lambda_s} \right)$$ (4)

Both stokes and anti-stokes are forms of inelastic scattering and despite the fact that the most dominant form of scattered light is of the elastic fraction, the inelastic fraction, which comprises only one out of every 10^6-10^8 photons, yields the wealth of information concerning the molecules being studied [5]. This information can be translated into a spectral signature unique to the particular material [6].
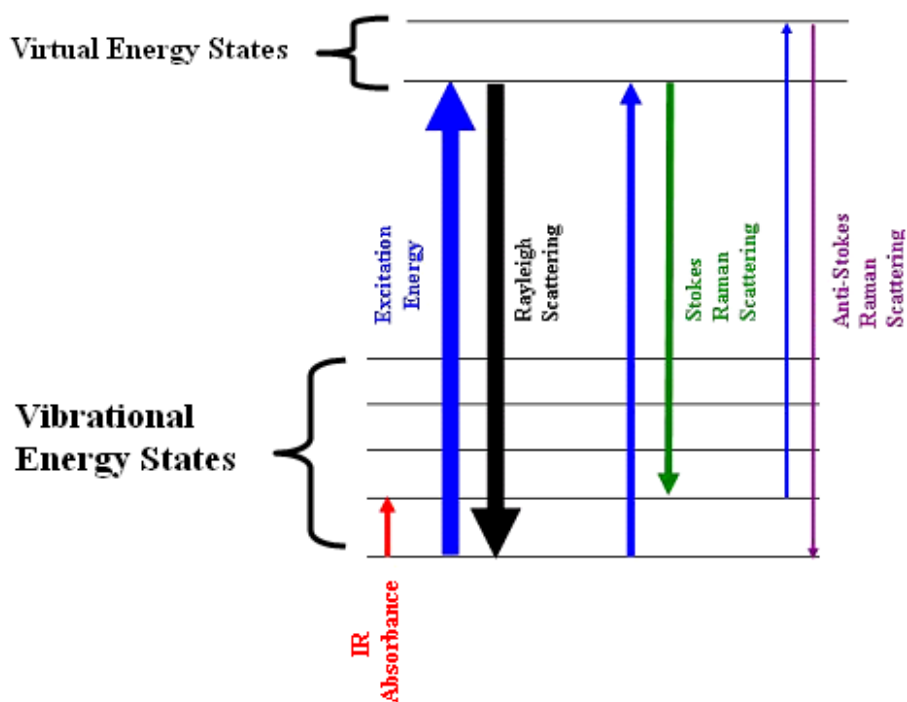
Figure 7. Energy levels and light scatterings involved in Raman spectroscopy [5].

As the technology regarding RS has improved and evolved, the analyzing power and breadth of substances analyzed has increased while the system's profile and physical footprint have decreased which has been demonstrated by a wave of portable handheld RS devices that have entered the market. Representative RS schematic, traditional, and portable device images are depicted in **Figures 8, 9, and 10**, respectively.
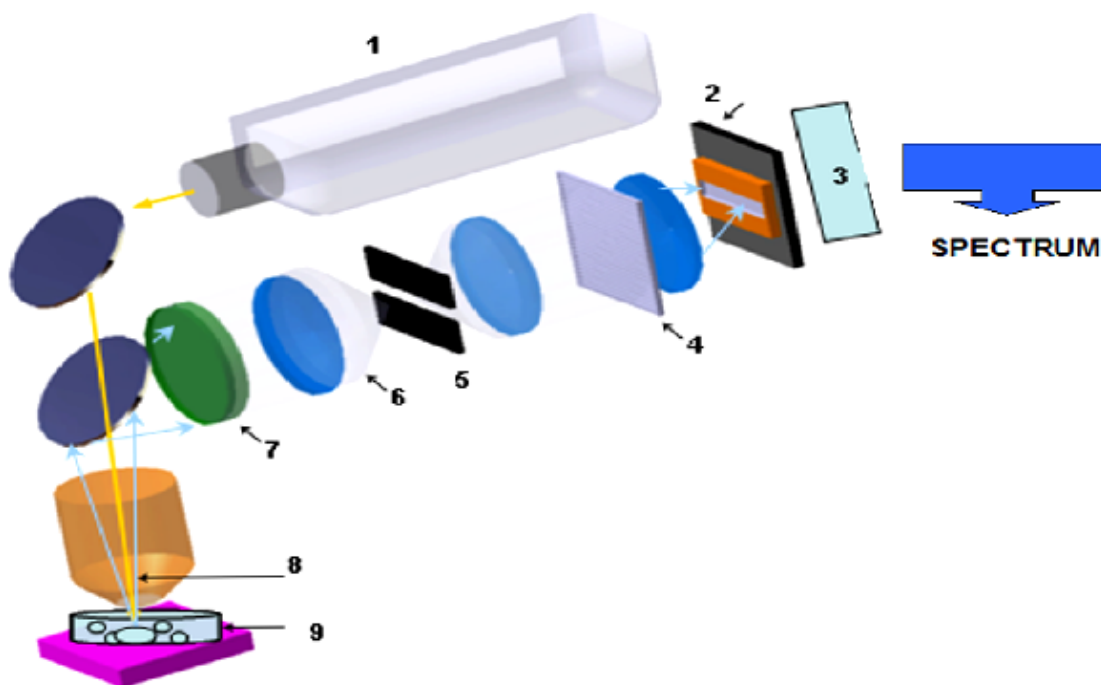
Figure 8. General schematic for Raman spectroscopic analyzer. 1-laser; 2-detector; 3-charge-coupled device; 4-diffraction grating; 5-slit; 6-Raman scattered light; 7-Rayleigh filters; 8-scattered light; 9-sample with lymphocyte culture.
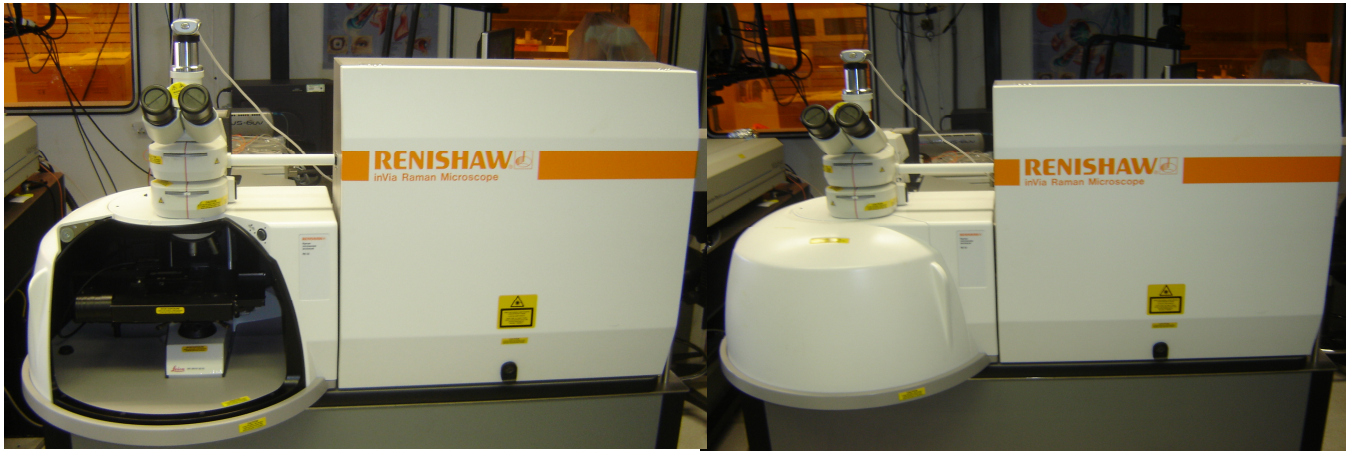
Figure 9. Image of Renishaw Raman Spectroscopic analyzer with open (left) and closed (right) microscope hood.

Figure 10. Portable Raman spectroscopic devices. (Left) MiniRam, (center)

MiniRam II (B&W Tec), and (right) InPhotote (InPhotonics)

Chapter 4.2- Biologic Applications of Raman Spectroscopy

The RS quantitative analysis of biologic materials, and more specifically, the individual components of these materials that could represent effective biomarkers, is complicated by several factors that are indissoluble from the biologic nature of these materials. First, nearly all biologic/biochemical material from pure water to living cells emit fluorescence at certain wavelengths. This fluorescence, which is usually at much greater intensity than peaks of interest, makes component analysis difficult. In general, incident photon wavelengths that yield higher resolution also demonstrate a greater tendency toward fluorescence. This spectral interference can be partially avoided by choosing the proper bathing media and by utilizing multi-spectral analysis and wavelengths that cause less fluorescence emission. In certain circumstances, peaks of interest may be located in regions of the spectrum that have negligible fluorescence, but this must be assessed on a case-by-case basis. Second, spectra of proteins and macromolecules are the sum total of the amino acid (AA) and subunit components. These elements exist on a continuum with extensive overlap of AA residues which results in, analytically, an averaged rather than discrete contribution. This challenge can be partially addressed by computer models [5] that can use spectral information derived from purified protein/subunit samples analyzed in isolation to deconstruct Raman peaks. However, this approach is limited and does not take into account the contribution of inter-protein interaction and its affect on the tertiary structure of proteins. To expand this example further, one can consider the living cell, which represents a biologic symphony containing countless carbohydrates, lipids, nuclear material, and proteins that scatter light at different intensities. The presence of these variable intensities makes it extremely difficult to isolate the contribution of one component and truly gauge its significance to the overall structure of the material being studied. This latter notion of structural significance can be

illustrated more simplistically if one were to consider a bottle made of a polymer which contains sulfur [5]. Polymers are weak Raman scatterers while sulfur is a strong scatterer. If the bottle was analyzed using RS, the spectrum would be dominated by sulfur peaks. However, the abundance of these peaks does not imply that the polymer is made predominately of sulfur molecules. The principles of this example can be extracted and applied to the study of living cells. If the structural significance of only two organic molecules contained in a matrix, the bottle, can be misinterpreted, then one can imagine the potential pitfalls that a cell, which has myriad of molecules in a multifaceted matrix, can present. Care should be taken when drawing conclusions about the global structure of a biologic or biochemical sample. Lastly, the living cell is susceptibility to heat, fungal/bacterial contamination, and damage due to excessive handling. These perturbations can significantly change the spectral signatures and make reproducibility of results problematic. For the most part, these issues can be addressed through proper experimental design and although quantitative analysis of the components in a biological system has posed unique challenges, the proper experimental design, ancillary resources (i.e. peak assignment databases for purified sample and analyzing software), and careful interpretation, has allowed RS to be developed into a valuable tool for the identification of biomarkers important to disease conditions. This can be illustrated by the success of RS in the areas of cellular biology, pathogen detection, and oncological identification [7-13]. Germaine to these studies has been the observation that RS is effective at quantifying differences and characteristics of individualized cells and their components. These Raman shifts can imply specific information concerning the cellular composition, cell surface biologic topography, and underlying biomolecular processes. The breadth of potential analysis carried out by RS can be further appreciated when considering that Takai and colleagues [14] were able to demonstrate the use of RS in characterizing cytotoxic

granules *within cells* while Notingher and others [15] demonstrated its utility in identifying specific peaks, 788 cm^{-1} and 1000.43 cm^{-1}, which reliably differentiated viable from nonviable *whole cells*. These observations were made possible by correlating the molecular-based signatures with the biological processes of DNA/RNA, carbohydrates, lipids, and protein alteration which occur on a cellular level [16, 17].

For this specific investigation of AR detection, the high resolution of RS was utilized to quantify the aforementioned cell surface receptor differences (see **Section 2.1 The Immunologic Basis of Renal Allograft Rejection**) between activated and non-activated T lymphocytes. In addition to its high resolution, RS offers many novel attributes that make it a potentially effective diagnostic tool. One of these attributes is that the system can be completely automated and contained in a device small enough to fit on the table-top in the clinical setting. This eliminates the need for specially-trained staff or large infrastructures/laboratories for processing of samples, two requirements that hampered previously-proposed noninvasive methods. In addition, RS affords rapid analysis (measurements can be completed in less than 10 minutes) and requires minute amounts of sample (blood or urine) to produce specific signatures. Unlike infrared spectroscopy, RS does not require the operator to match the frequency of the incident photon to that of the vibration of the particular molecule in order to promote that molecule to a vibrational excitation state and unlike flow cytometry, RS does not require expensive antibodies to carry out analysis. The implication of these observations is that there is less processing and pretest manipulation of samples using a RS system [5]. All of these attributes suggest that this technologic platform can be developed into a highly accurate, noninvasive diagnostic tool for AR.

REFERENCES

1. Singh R. C. V. 2002. Raman and the Discovery of the Raman Effect. Physics in Perspective l4 (4).

2. Gardiner DJ and Graves PR. 1989. Practical Raman Spectroscopy. Berlin: Springer.

3. J. Fischer. 2005. George Placzek - an unsung hero of physics. Cern Courier 45(7).

4. Schrader, B. 1995. Infrared and Raman Spectroscopy. New York. VCH Publishers Inc. Chapter 4.

5. Smith E, Dent G. 2005. Modern Raman Spectroscopy: A practical approach. West Sussex, England. Wiley. Chapters 1-3.

6. Morris, M.D. 1992. Applied Laser Spectroscopy. Andrews, D.L. Ed. New York. VCH Publishers Inc. Chapter 6.

7. Crow P, J. S. Uff J. A. Farmer M. P. Wright, and N. Stone. 2004. The use of Raman spectroscopy to identify and characterize transitional cell carcinoma in vitro. BJU Int. 93: p. 1232–1236.

8. Frank, C. J., R. L. Mccreery, and D. C. B. Redd. 1995. Raman spectroscopy of normal and diseased human breast tissues. Anal Chem 67: p. 777–783.

9. Boyum A. 1976. Separation techniques for mononuclear blood cells. HLA Typing: Methodology and Clinical Aspects Vol. I: p. 2

10. Mittal KK, Fotino M and Menon AK. 1981. Isolation and purification of peripheral blood. In: Zachary AA and Bruan WE, ed. AACHT laboratory Manual Am Associ For Clinical Histocompatibility Testing. NY, 1-2-1.

11. Chan D, Theodore Z, Stephen L, Ko I. 2006. Micro-Raman spectroscopy detects individual neoplastic and normal hematopoietic cells. Biophysical Journal 90. p. 648-656.

12. Xun-Ling Yan, Rui-Xin Dong, Lei Zhang, Zong-Wang Zhang. 2005. Raman spectra of single cell from gastrointestinal cancer patients. World J Gastroenterol 11(21): p. 3290-3292.

13. Lyng F, Faolain E, Conroy J, Meade A, Knief P, Duffy B, Hunter M, Byrne J, Kelehan P, Byrne H. 2007. Vibrational spectroscopy for cervical cancer pathology, from biochemical analysis to diagnostic tool. Experimental and Molecular Pathology 82. p. 121-129.

14. Yoshiaki Takai, Takashi Masuko, Hideo Takeuchi. 1997. Lipid structure of cytotoxic granules in living human killer T lymphocytes studied by Raman microspectroscopy. Biochimica et Biophysica Acta 1335. p. 199–208.

15. I. Notingher, S. Verrier, S. Haque, J. M. Polak, L. L. Hench. 2003. Spectroscopic Study of Human Lung Epithelial Cells (A549) in Culture: Living Cells versus Dead Cells. Biopolymers (Biospectroscopy), 72, p. 230–240.

16. Benevides J. M., and G. J. Thomas. 1983. Characterization of DNA structures by Raman spectroscopy: high-salt and low-salt forms of double helical poly (dG-dC) in H2O and D2O solutions and application to B, Z and A-DNA. Nucleic Acids Res. 11:5747–5761.

17. Abe, M., T. Kitagawa, Y. Kyogoku. 1978. Resonance Raman spectra of octaethylporphyrinato-Ni (II) and meso-deuterated and 15 N substituted derivatives. II. A normal coordinate analysis. J Chem Phys 69: p. 4526-4534**.**

CHAPTER 5- RAMAN SPECTROSCOPIC DIFFERENTIATION OF ACTIVATED VERSUS NON-ACTIVATED T LYMPHOCYTES: AN IN VITRO STUDY OF AN ACUTE ALLOGRAFT REJECTION MODEL [1]

Chapter 5.1- Introduction

As mentioned previously, we hypothesize that the differentiation of activated and non-activated (resting and inactivated) T lymphocytes can be accomplished by using RS analysis of cell surface receptors. The goal of the study presented in this chapter was to investigate initial spectral signature differences between activated (alloreactive) and non-activated T lymphocytes and to assess the effectiveness of an *in vitro* cellular model that will allow the necessary analysis on a RS platform.

Chapter 5.2- Materials and Methods

5.2.1- Cellular Preparation

Following approval from the Wayne State University Human Investigation Committee (HIC; **Appendix F**), mononuclear cells were obtained using freshly drawn (within 3 hours of experimentation) sodium-heparinized venous blood collected from healthy individuals and separated according to density via high molecular weight sucrose polymer (ficoll) as described by Boyum [2]. The resultant cells were washed three times using Hank's balanced salt solution (HBSS, Invitrogen, Carlsbad, CA) and suspended in McCoy's solution/5% fetal calf serum (Biofluids, Rockville, MD) prior to T lymphocyte isolation. B lymphocytes were subsequently removed by negative selection using FluoroBeads-B immunomagnetic beads and magnetic sorter (One Lambda, Canoga Park, CA). This process was repeated twice with chilled phosphate buffered saline (PBS; Invitrogen, Carlsbad, CA) washings used to suspend cells between magnetic separations. Cell viability was >98% as checked by vital dye exclusion. T lymphocyte

enriched samples were suspended in complete medium and aliquoted for subsequent experimentation.

5.2.2- Peripheral Blood T Lymphocyte Samples

Three distinct T lymphocyte sample groups were created for the study, consisting of activated, inactivated, and resting T lymphocytes. The activated T lymphocyte samples were the product of a two-way mixed lymphocyte culture (MLC) as described by Dupont and colleagues [3]. The inactivated group was created using T lymphocyte/stimulator samples from two unrelated individuals that were pretreated for 20 minutes with Mitomycin C (0.025 mg of Mitomycin C (0.5 mg/ml) to each 1 ml of cell suspension) at 37°C and washed twice using HBSS prior to start of MLCs. Efficacy of Mitomycin C was verified using double inactivation control cultures which were run in parallel. Finally, the resting T lymphocyte sample group was defined as T lymphocytes obtained by methods described previously, which were neither stimulated via MLC nor inhibited by Mitomycin C treatment. Following MLC but prior to RS analysis, B cells were removed by negative selection using FluoroBeads-B immunomagnetic beads and magnetic sorter (One Lambda, Canoga Park, CA) while monocytes/macrophages were removed via steel wool columns to ensure that these signatures were not obtained erroneously. All cultures were incubated at 37°C in 5% CO_2 in parallel over a 7-day period with RS testing, antibody analysis, and viability assays carried out daily.

5.2.3- Independent Verification of Activation/Inactivation via Antibody Staining

Activation and inactivation of representative aliquots were verified using FastImmune anti-Hu-Il-2 FITC/CD69 PE/CD4 Per CP- Cy5.5/CD3 APC (Becton Dickinson, San Jose, CA), with 94% of MLC (activated) and 100% of Mitomycin C-treated (inactivated) T lymphocytes

staining positive and negative, respectively, using protocols described elsewhere [4]. In addition, there was no detected activation due solely to physical handling of lymphocytes. Stained cells were viewed using a Nikon Eclipse TE 2000-U inverted microscope with images being captured and processed using Metavue 6.2r5 software (Downingtown, PA).

5.2.4- Raman Spectroscopic Analysis

Prior to analysis, all samples were washed with PBS (Invitrogen, Carlsbad, CA). Cells were allowed to settle within the analysis reservoir placed on a leveled microscope stage. Only rounded, non-adhered, isolated and individualized T lymphocytes were selected for study. Each sample was analyzed using identical protocol and spectroscopic parameters. Using an enhanced video imaging system, T cells were aligned in the laser target area so that the focus point was centered on the lymphocyte. Images were captured before and after each measurement with no noted cell shifting or destruction observed. Wire 2 software (Renishaw plc, Old Town, United Kingdom) was utilized in conjunction with the Raman system for quantitative measurement. Raman spectroscopic measurements were conducted using a Renishaw InVia 2000 microscope-spectrometer with a Leica 63X water immersion objective (NA= 1.20). Due to the complexity of biological structures which can embody numerous vibrational modes, two different excitation wavelengths were used in this study. T lymphocytes were analyzed using both 785 nm (red) diode and 514.5 nm (green) Ar^+ excitation wavelengths. Laser power was set at 50% (8-12 mW) for a 2-4 μm laser spot size. Spectra were collected in the backscattering geometry with a 10 second integration time over a range of 500 to 1700 cm^{-1}. The theoretical spectral resolution was ~ 4 cm^{-1}. A schematic of the Raman spectroscopic system is depicted in **Figure 8**.

5.2.5- Statistical Analysis

Prior to statistical analysis, all data was checked for various types of noise. There was no significant fluorescence observed for the 785 nm wavelength excitation. However, with the 514.5 nm excitation, Raman spectral data showed fluorescence uniformly increasing over the entire range of Raman shift. This fluorescence was subtracted out using a modified cubic-spline algorithm that required no *a priori* knowledge of the spectra. In addition, a median filter was applied to raw data to eliminate any cosmic ray or spikes in the data. The Raman spectra from all data contained 1184 data points. To determine the independent variations in the intensity which basically represents different pathological states in the sample, we used principal component analysis (PCA) to reduce dimensionality in the data. We found that seven eigenvectors were able to capture more than 97% of total variance in the data. Student's t-test was utilized to further quantify differences in peak ratios. The data were further analyzed for the presence of various independent groups using discriminant function analysis (DFA) with the aforementioned eigenvectors as input variables. Graphical and quantitative analysis of data was accomplished using SPSS version 15 software (Statistical Software, Chicago, IL).

Chapter 5.3- Results

5.3.1- Raman Spectroscopic Results - Green (514.5 nm) Laser

A total of 23 activated, 12 inactivated, and 20 resting T lymphocytes were examined. A representative mean Raman spectrum of resting T lymphocytes is depicted in **Figure 11** with proposed peak assignments for 1182 cm^{-1} and 1195 cm^{-1} positions shown in **Appendix B**. There was no observed cellular disruption during measurements, and after comparison of activated and non-activated (resting and inactivated) spectra from 500-1700 cm^{-1}, qualitative differences were seen at the 1182 cm^{-1} and 1195 cm^{-1} positions.

Representative activated and inactivated T lymphocyte spectra are depicted in **Figures 12A** and **12B**, respectively. Ratios of the 1182 cm^{-1} and 1195 cm^{-1} peaks were determined by comparison of amplitudes with respect to a designated baseline depicted by a dashed line in the figures. The average peak ratios for the 1182 cm^{-1} and 1195 cm^{-1} positions for the activated, inactivated, and resting T lymphocyte groups were 0.98 ± 0.04, 1.13 ± 0.10, and 1.10 ± 0.05, respectively. Significant differences in peak ratios existed between activated and resting as well as between activated and inactivated T lymphocyte groups ($p = 0.001$ and $p = 0.0001$, respectively). There was a trend observed in the differences between inactivated and resting T lymphocytes ($p = 0.07$).

A summary of all RS data collected with 514.5 nm excitation for activated, inactivated, and resting T lymphocytes is shown in **Figure 13.** Based upon the distribution of raw data, 3 distinct sectors were assigned for grouping purposes: Sector I, inactivated T cells; Sector II, activated T cells; Sector III, resting T cells. 95.7% of activated T lymphocytes clustered in Sector II, with the remaining 4.3% clustering in Sector I. One hundred percent of inactivated T lymphocyte samples clustered in Sector I, while 60% of the resting T lymphocytes were found in Sector III, and 40% in Sector I. This data supports a 96% Sensitivity (defined here as the ability to detect T cell activation) and a 100% Specificity (defined here as the ability to detect non-activated T cells or rule out T cell activation).

Figure 11. Raman spectroscopic analysis of T lymphocytes using 514.5 nm laser over a range of 500-1700 cm^{-1}.

Representative T cell (inset a) demonstrating cellular integrity following analysis.

(*) Indicates area of focus containing the 1182 and 1195 cm^{-1} peaks.

Figure 12. (A) Raman spectroscopic analysis of 1182 cm^{-1} (*) and 1195 cm^{-1} (^) peaks for activated T lymphocytes at the 514.5 nm wavelength. Inset a shows independent verification of activation via anti-IL-2/CD69/CD4/CD3 antibody staining. (B) Spectroscopic analysis of inactivated T lymphocyte, with inset b showing non-activation. Ratios determined by amplitude with respect to designated baseline (dashed line).

Figure 13. Discriminant function analysis of T lymphocytes at 514.5 nm wavelength plotted without (A) and with (B) assigned sectors. Sectors I, II, and III correspond to inactivated, activated, and resting samples, respectively.

5.3.2- Raman Spectroscopic Results - Red (785 nm) Laser

A total of 28 activated, 16 inactivated, and 15 resting T lymphocytes were examined. A representative mean Raman spectrum of resting T lymphocytes is depicted in **Figure 14**. There was no observed cellular disruption following laser exposure.

The average peak ratios for the 1182 cm^{-1} and 1195 cm^{-1} positions for the activated, inactivated, and resting T lymphocyte groups were 0.93 ± 0.05, 1.15 ± 0.10, and 1.09 ± 0.09, respectively. Representative activated and inactivated T lymphocyte spectra are depicted in **Figures 15A** and **15B,** respectively. Significant differences in peak ratios existed between activated and inactivated as well as between activated and resting T lymphocytes ($p = 0.001$ and $p = 0.006$, respectively). In contrast, there was only a trend seen in differences between inactivated and resting T lymphocytes ($p = 0.08$). **Figure 16** demonstrates the DFA plot for activated, resting, and inactivated T lymphocyte Raman spectral data collected using the 785 nm wavelength. 89.3% of the activated T lymphocytes grouped into Sector II, with 3.6% falling into Sector I and 7.1% clustering into Sector III. 93.8% of the inactivated T lymphocytes were found in Sector I, while 6.2% marginalized into Sector III. 86.6% of the resting T lymphocytes were found in Sector III with 13.4% clustering into Sector I. This data supports an 89.3% Sensitivity and a 93.8% Specificity.
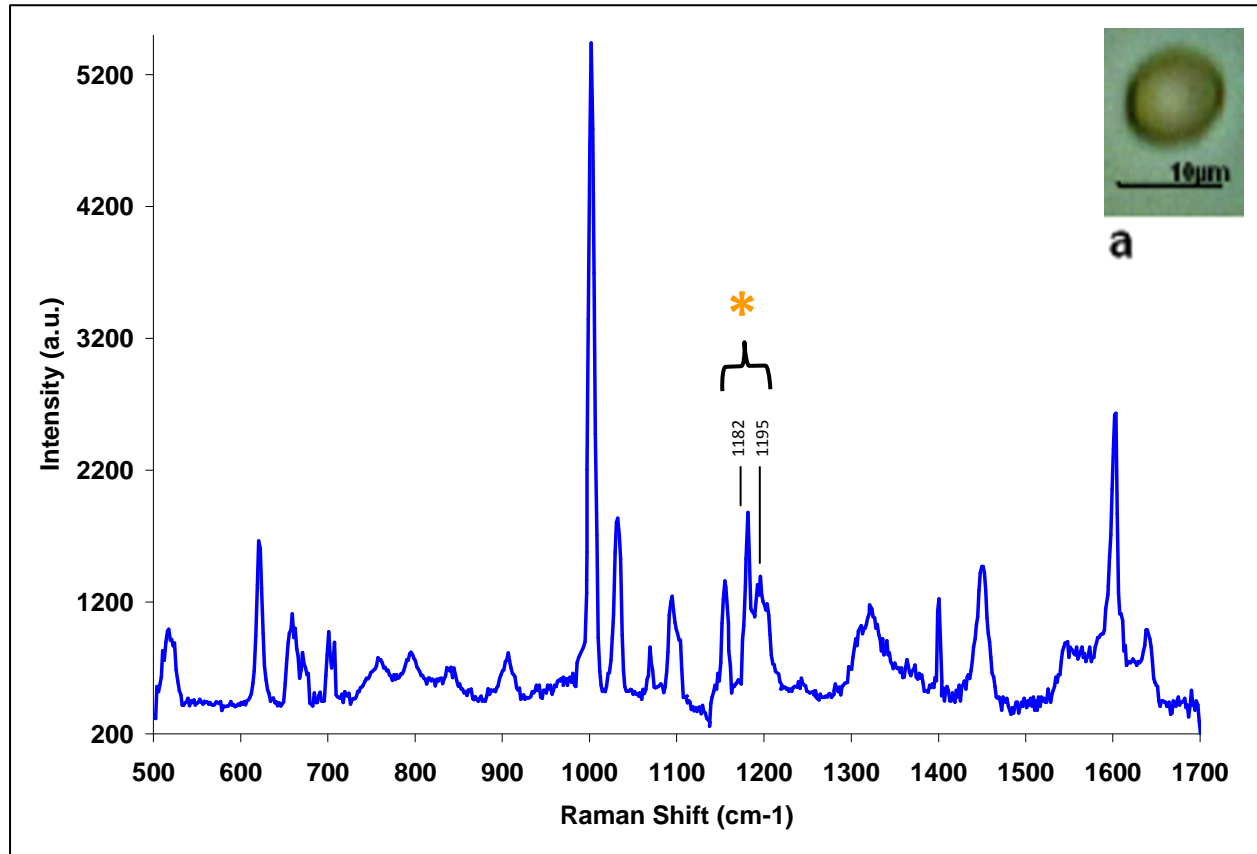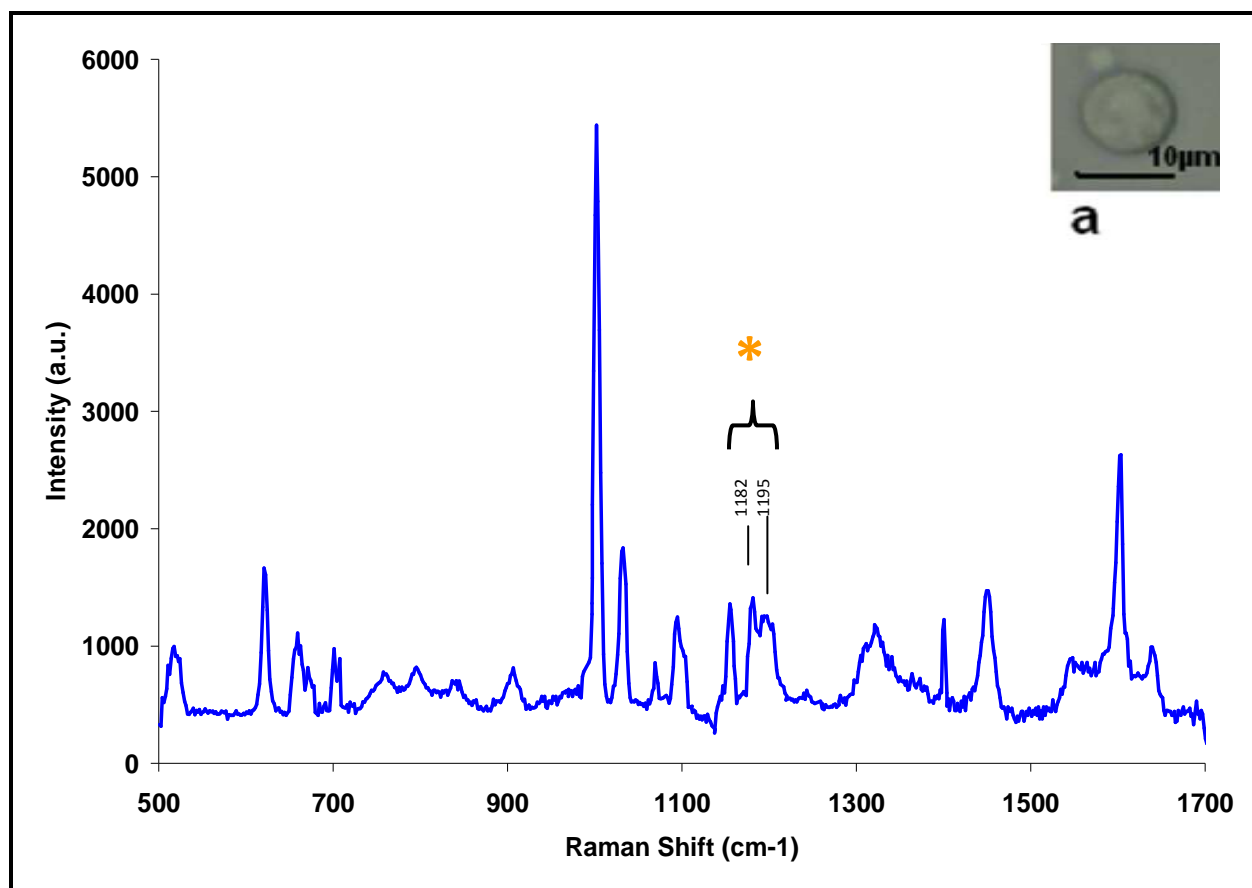
Figure 14. Raman spectroscopic analysis of T lymphocytes using 785 nm laser with range of 500-1700

cm^{-1}. Representative T cell (Inset a) demonstrating cellular integrity following analysis.

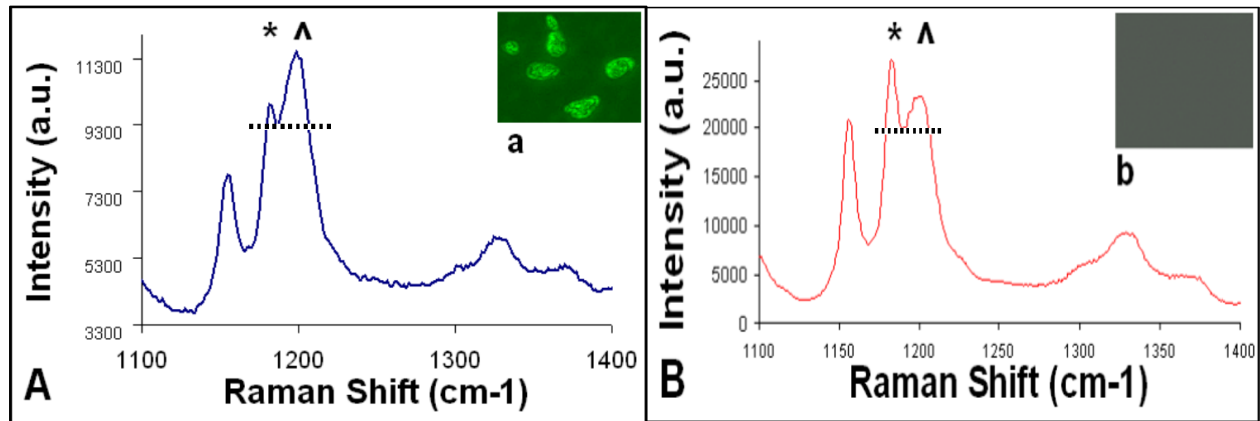(*) Indicates area of focus containing the 1182 and 1195 cm^{-1} peaks.
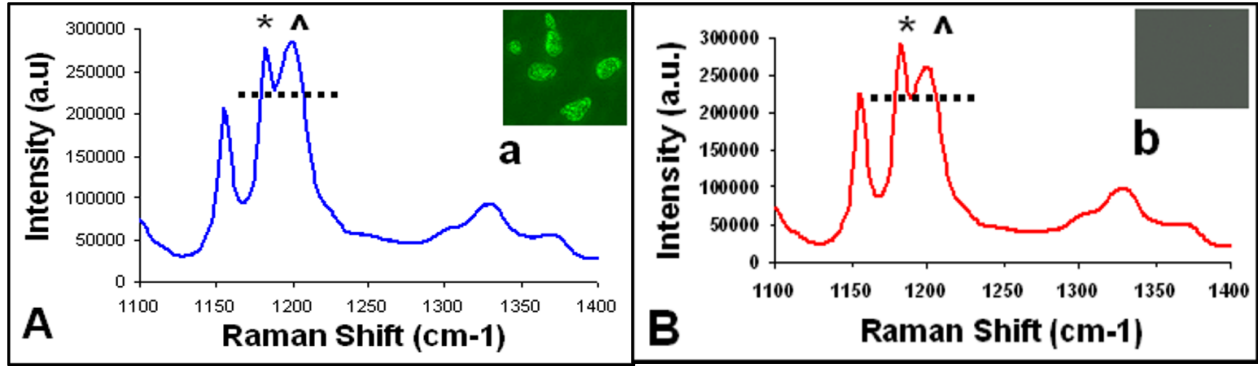
Figure 15. (A) Raman spectroscopic analysis of 1182 cm^{-1} (*) and 1195 cm^{-1} (^) peaks for activated T lymphocytes for the 785 nm wavelength. Inset a shows independent verification of activation via anti-IL-2/CD69/CD4/CD3 antibody staining. (B) Spectroscopic analysis of inactivated T lymphocyte with inset b demonstrating non-activation. Ratios determined by amplitude with respect to designated baseline (dashed line).
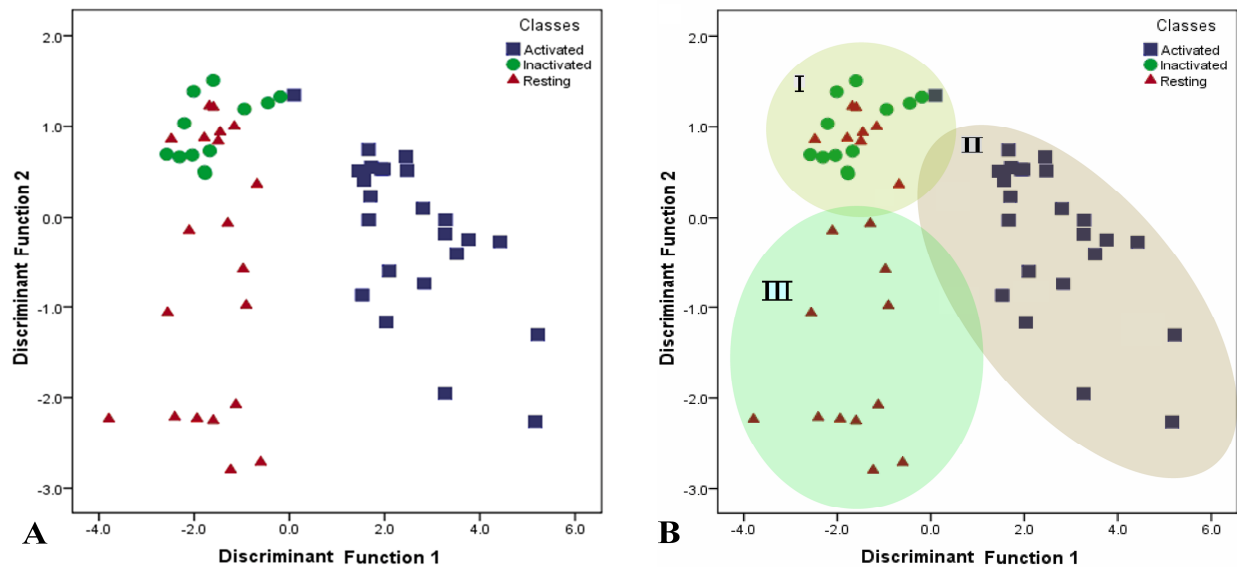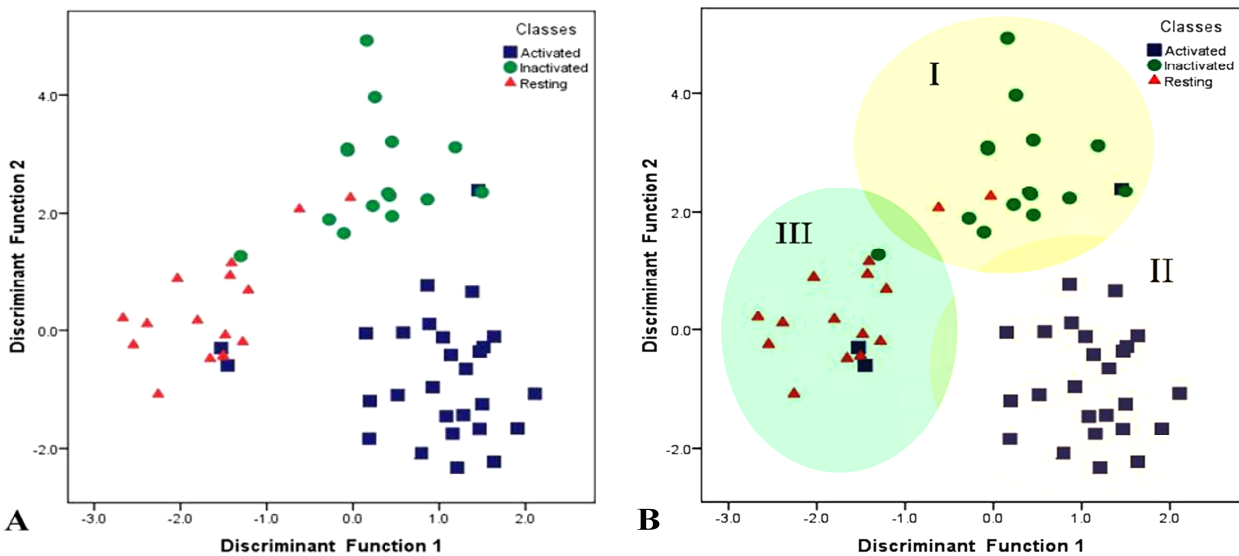

Figure 16. Discriminant function analysis of T lymphocytes at 785nm wavelength plotted without (A) and with (B) assigned sectors. Sectors I, II, and III correspond to inactivated, activated, and resting samples, respectively.

Chapter 5.4- Discussion

The process of T lymphocyte activation spans from initiation of the genetic apparatus via immunospecific transcription factors to the up-regulation of glycoproteins and lipid turnover on the T lymphocyte surface. In general, Raman peak assignments can be categorized as nucleic acid, carbohydrate, lipid, or protein in nature. Indeed, this process of activation encompasses all peak assignment categories and importantly, can be quantified by our RS system.

The purpose of this study was to utilize RS to establish spectral differences between activated and non-activated T lymphocytes. Initial qualitative comparison of activated and non-activated T lymphocytes yielded notable foci at five distinct positions in the Raman spectrum: 628 cm^{-1}, 788 cm^{-1}; 1000.43 cm^{-1}; 1182 cm^{-1}; and 1195 cm^{-1}. Peaks at 628 cm^{-1}, 788 cm^{-1}, and 1000.43 cm^{-1} have been previously identified and described as markers for cellular viability [5]. However, a novel and distinct spectral difference in peak positions was observed at 1182 cm^{-1} and 1195 cm^{-1}. These differences, and more importantly their ratio to one another, have not been previously described.

The *in vivo* immunologic landscape concerning the activation of T lymphocytes exists on a continuum, with the breadth of the spectrum ranging from anergy to full activation [6]. The observation that a small subset of activated T lymphocytes in both the 514.5 nm and 785 nm cohorts were found in Sectors I and III, or the inactivated and resting T lymphocyte sectors, respectively, can be explained by the concept of anergy or the inability to up-regulate receptors of activation due to the absence of the co-stimulatory feedback, signal 2 (see **Section 2.1 Immunologic Overview** and **Figure 2**) [6]. *In vivo*, this process ideally prevents a T lymphocyte from reacting and clonally expanding in response to a self antigen without confirmation. To further address this issue and verify this phenomenon, we conducted a study to circumvent

anergy through a method of non-specific activation that is independent of MHC restriction (see **Chapter 6**). No inactivated T lymphocytes were found in Sector II. This important observation verifies the notion that although we would expect a small percentage of alloreactive T lymphocytes to fail to activate due to anergy, we would not expect a Mitomycin C-treated T lymphocyte to activate and thus falsely group with activated samples in Sector II. This also suggests that an eventual high specificity of RS can be achieved. This notion was tested and is addressed in **Chapter 6**.

Although the difference in average peak ratios between resting and inactivated T lymphocyte groups of both green and red lasers did not quite reach statistical significance, the trend toward difference depicted in the DFA plots were graphically apparent, allowing for discrimination. The exchangeability found between Sectors I and III that did not exist for Sector II suggests that there is a threshold of activation required to populate the T lymphocyte surface with a density of receptors necessary to create a distinct activation signature.

Based upon Raman spectra from excitation wavelengths 514.5 nm and 785 nm, average peak ratios, and DFA plots, there was a significant difference observed between the activated T lymphocyte group and the non-activated (resting and inactivated) T lymphocyte groups. When considering both wavelengths, the green laser demonstrated a higher resolution and tighter association of T lymphocytes to their designated sector, with 96% of activated T lymphocytes aggregating into Sector II (sensitivity) and 100% of inactivated T lymphocyte samples aggregating into Sector I (specificity). We utilized this observation in the planning of subsequent experiments in which we employed the 514.5 nm (green) laser exclusively.

REFERENCES

1. Brown KL, Palyvoda OY, Thakur JS, Nehlsen-Cannarella SL, Fagoaga OR, Gruber SA, Auner GW. 2009. Raman spectroscopic differentiation of activated versus non-activated T lymphocytes: an in vitro study of an acute allograft rejection model. J Immunol Methods 340(1):48-54.

2. Boyum, A. 1968. Isolation of leukocytes from human blood. Further observations methyl, cellulose, dextran, and ficoll as erythrocyte aggregating agents. Scand J Clin Invest 97 (Suppl):31.

3. Dupont, B., Hansen, J.A., Yunis, E.J. 1976. Human mixed-lymphocyte culture reaction: Genetic, specificity and biological implications. In: Advances in immunology, Academic Press, New York, 107.

4. Schwarting, R., Biedobitek, G., Stein, H. 1989. Cluster report: CD69. In: Knapp W, Dörken B, Gilks WR, et al, eds. Leucocyte Typing IV: White Cell Differentiation Antigens New York, NY: Oxford University Press: p. 428-432.

5. Notingher, I., Verrier, S., Haque, S., Polak, J.M., Hench, L.L. 2003. Spectroscopic Study of Human Lung Epithelial Cells (A549) in Culture: living cells versus dead cells. Biopolymers. Biospectroscopy 72, p. 230–240.

6. Janeway, C., Travers, P., Walport, M., Capra, J. 1999. T Cell Mediated Immunity. In: Austin, P., Lawrence, E. Immunobiology: The immune system in health and disease 4th edition. Garland Publishing, NY 510-514.

CHAPTER 6- DIFFERENTIATION OF ALLOREACTIVE VERSUS CD3/CD28 STIMULATED T LYMPHOCYTES USING RAMAN SPECTROSCOPY: A GREATER SPECIFICITY FOR NONINVASIVE ACUTE RENAL ALLOGRAFT REJECTION DETECTION [1]

Chapter 6.1- Introduction

In the preceding chapter, (**Ch. 5**) the notion of sensitivity (the ability to distinguish activated from non-activated T lymphocytes) was explored. Despite the establishment of RS as a methodology to identify T lymphocyte activation, the specificity of this system, defined here as *the ability to distinguish signatures of two sets of T lymphocytes that are activated by different stimuli*, still required examination. This study focuses on spectral signature differences of alloantigen-activated and CD3/CD28-activated T lymphocytes. We hypothesize that the RS signatures of T cells activated via these two methodologies will differ significantly.

Chapter 6.2- Materials and Methods

6.2.1- Alloantigen-activated T Lymphocyte Preparation

Prior approval for the study was obtained from the Wayne State University HIC. Mononuclear cells were obtained from healthy volunteers using protocol described previously (see **section 5.2.2**).

Three distinct T cell sample groups were created for the alloantigen-activated T cells: 1. activated; 2. inactivated; and 3. resting T lymphocytes. The activated T lymphocyte samples were created via a two-way MLC as described previously (see **section 5.2.2**). T cell activation was confirmed by CD69 directed flow cytometry (**Appendix C**) [2, 3]. The inactivated group was created by utilizing T lymphocyte/stimulator samples from two non-related individuals which were pretreated with Mitomycin C as previously described (see **section 5.2.2**). Finally, the

resting T lymphocyte group consisted of lymphocytes that were neither stimulated via MLC nor inhibited by Mitomycin C treatment. These cells were the product of CD69 negative sorting via flow cytometry [2, 3]. All cultures were incubated at 37 degrees Celsius in 5% CO_2 in parallel over a 7-day period, with RS, antibody, and viability analysis carried out daily.

6.2.2- Non-specific Antigen Model of Activation

T lymphocytes were isolated directly from peripheral blood and urine using a Dynal T cell negative isolation kit (Invitrogen, Canoga Park, CA). In order to model a nonspecific process of activation, a CD3/CD28-coated Dynal bead system (Invitrogen, Canoga Park, CA) was utilized to cross-link cell membrane molecules. This consisted of T lymphocytes incubated with beads (bead volume titrated to correspond to 3 beads for every T cell at a concentration of 1 x 10^7 cells per volume) in complete media containing recombinant interleukin 2 (50U/ml). The CD3/CD28 beads were removed from T lymphocytes via high efficiency magnetic sorter prior to Raman analysis.

6.2.3- Independent Verification of Activation/Inactivation

Independent of RS analysis, the activation status of all samples was verified by antibody staining and flow cytometry (**Appendix C**). For the alloreactive and CD3/CD28 stimulated samples, activation status was assessed using a monoclonal antibody, CD69 (FastImmune, Becton Dickinson, San Jose, CA), as described elsewhere [4]. Stained cells were viewed using a Nikon Eclipse TE 2000-U inverted microscope, with images captured and processed with Metavue 6.2r5 software (Downingtown, PA).

6.2.4- Raman Spectroscopic Analysis

Lymphocyte selection, Raman measurement parameters, and cellular integrity verification was carried out as previously described (see **section 5.2.4**). To provide for reference/control spectral peaks, both pure CD3/CD28 beads and T lymphocytes that were not subjected to magnetic sorter (T cells still bound with beads), were analyzed. Wire 2 software (Renishaw plc, Old Town, United Kingdom) was utilized in conjunction with the RS system for quantitative measurement.

RS measurements were conducted using a Renishaw InVia 2000 microscope-spectrometer with a Leica 63 X water immersion objective (NA = 1.20). T lymphocytes were analyzed using the 514.5 nm (green) Ar^+ excitation wavelength. Laser power was set at 50% (8-12 mW) for a 2-4 μm laser spot size. Spectra were collected in the backscattering geometry with a 10 second integration time over a range of 600 to 1700 cm^{-1} with a spectral resolution of 4 cm^{-1}.

6.2.5- Statistical Analysis

Prior to statistical analysis, all data were checked for various types of noise. Spectral data demonstrated uniformly increasing fluorescence over the entire range of Raman shift. This was subtracted out using a modified cubic-spline algorithm requiring no *a priori* knowledge of the spectra. In addition, a median filter was applied to the raw data which eliminated cosmic ray and spikes. PCA was used to reduce dimensionality in the data. Chi square or *Student's* T test was utilized as appropriate to further quantify differences in peak ratios and peak magnitudes with additional quantitative differences determined by DFA. Graphical and quantitative analysis of data were accomplished using SPSS version 15 software (Statistical Software, Chicago, IL).

Chapter 6.3- Results

6.3.1- CD3/CD28-activated versus Inactivated T Lymphocytes

A total of 75 CD3/CD28-activated and 75 inactivated T cells were analyzed using the 514.5 nm excitation wavelength. Systematic review of samples revealed no cellular disruption following laser exposure. Qualitative comparisons of activated and inactivated spectra demonstrated differences at 903 cm^{-1}, 1031 cm^{-1}, 1069 cm^{-1}, 1093 cm^{-1}, 1155 cm^{-1}, 1326 cm^{-1}, and 1449 cm^{-1} peak positions (**Figure 17**). Quantitative analysis of these shifts demonstrated differences in peak magnitudes at all positions except for 628cm^{-1}, 788 cm^{-1}, and 1002 cm^{-1} (**Table I, Figure 18A-E**), which have been shown in previous studies to correlate with cellular viability [5]. Moreover, the CD3/CD28-activated and inactivated groups showed significant differences in peak ratios at the 1182:1195 cm^{-1} position (**Table I, Figure 19**).

Figure 17. Superimposed mean Raman spectra from inactivated (red) and CD3/CD28-activated T lymphocytes

annotated with (*) foci of significant differences and (^) markers of cellular viability [5].
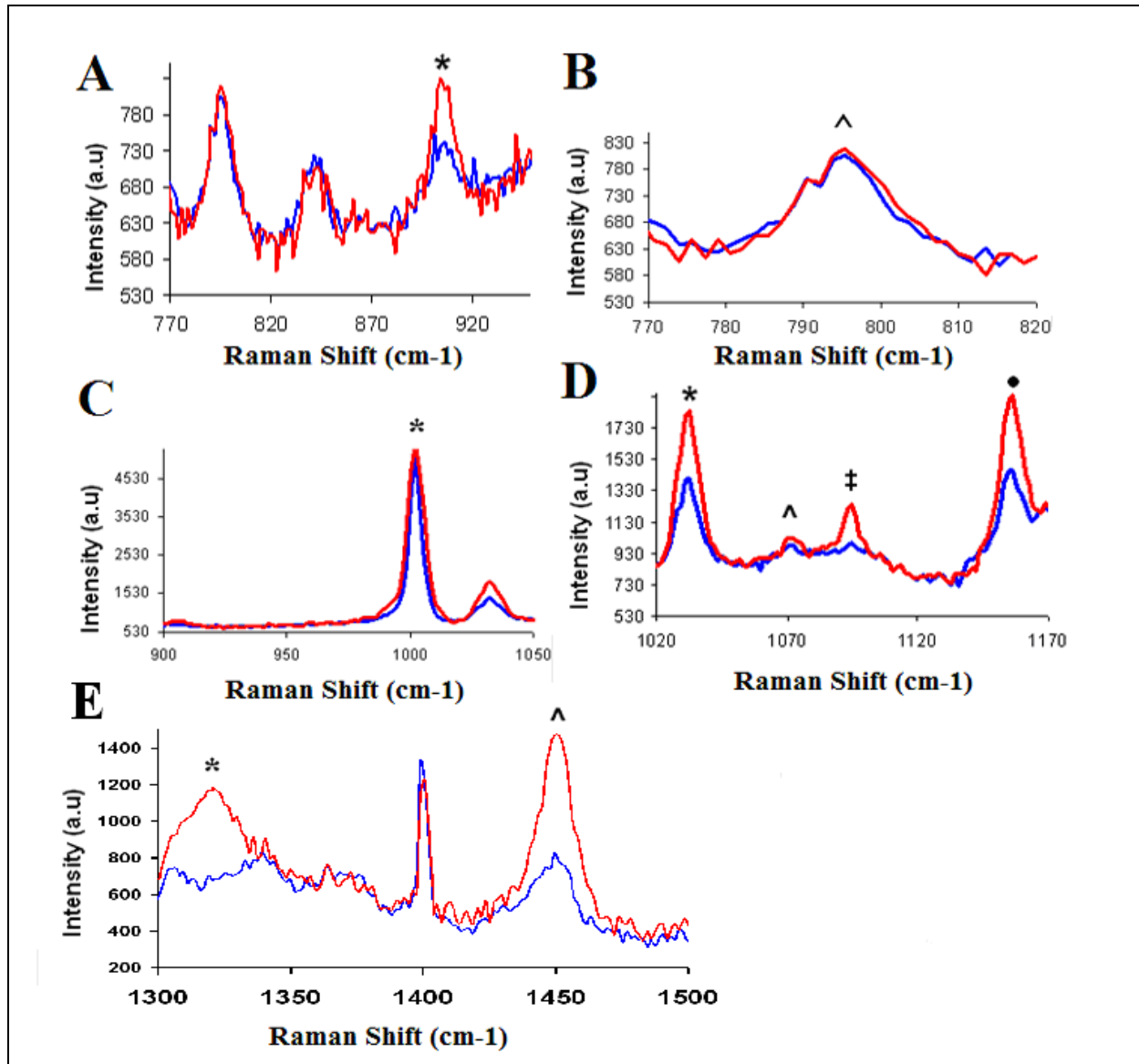
Figure 18. Raman spectra of inactivated (red) and CD3/CD28-activated (blue) T lymphocytes demonstrating differences in peak magnitudes (insets A, D, and E) and comparable peaks at viability markers (Insets B and C). Annotations within insets: Inset A- (*) 903 cm^{-1}; Inset B- (^) 788 cm^{-1}; Inset C- (*) 1002 cm^{-1}; Inset D- (*) 1031 cm^{-1}, (^) 1069 cm^{-1}, (‡) 1093 cm^{-1}, (•) 1155 cm^{-1}; Inset E- (*) 1326 cm^{-1}, (^) 1449 cm^{-1}. Note: These focused spectral regions are from T lymphocytes represented in **Figure 17.**
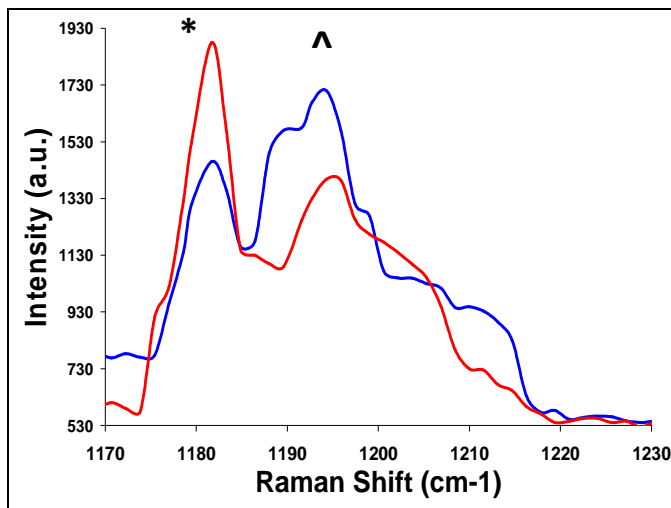
Figure 19. Raman spectra of inactivated (red) and CD3/CD28-activated T lymphocytes demonstrating differences in (*) 1182 cm^{-1} and (^) 1195 cm^{-1} peaks.

6.3.2- CD3/CD28-activated versus Alloantigen-activated T Lymphocytes

A total of 46 CD3/CD28-activated and 40 alloantigen-activated T cells were analyzed with summary comparison spectra shown in **Figure 20**. When comparing these groups, they differed significantly at the 903 cm^{-1}, 1031 cm^{-1}, 1093 cm^{-1}, 1155 cm^{-1}, 1326 cm^{-1}, and 1449 cm^{-1} positions. However, there was no difference when analyzing the peak ratio at the 1182:1195 cm^{-1} position (**Figure 20, Table I**). DFA of the Raman spectral data for CD3/CD28-activated and alloantigen-activated T cell groups is summarized in **Figure 21**. There was 100% accuracy when using the activation signature to separate these groups.
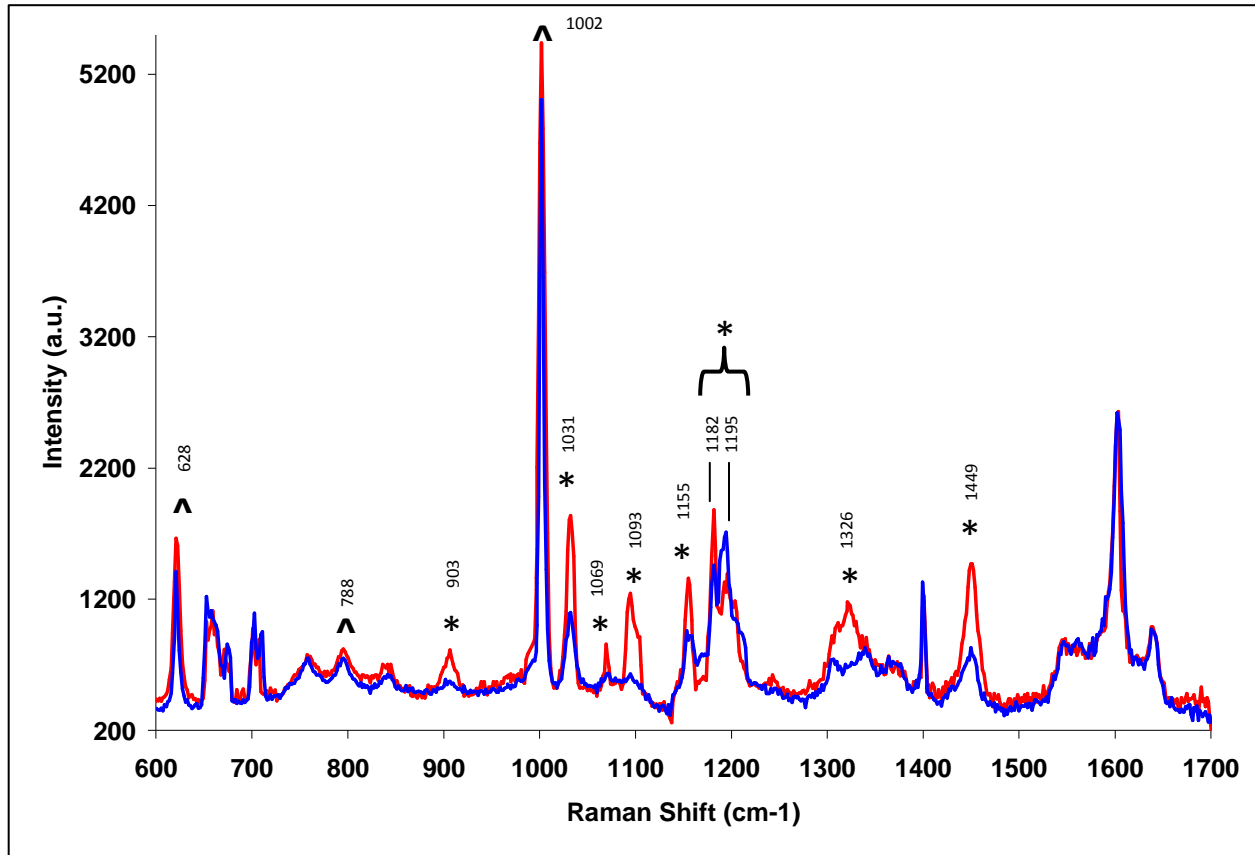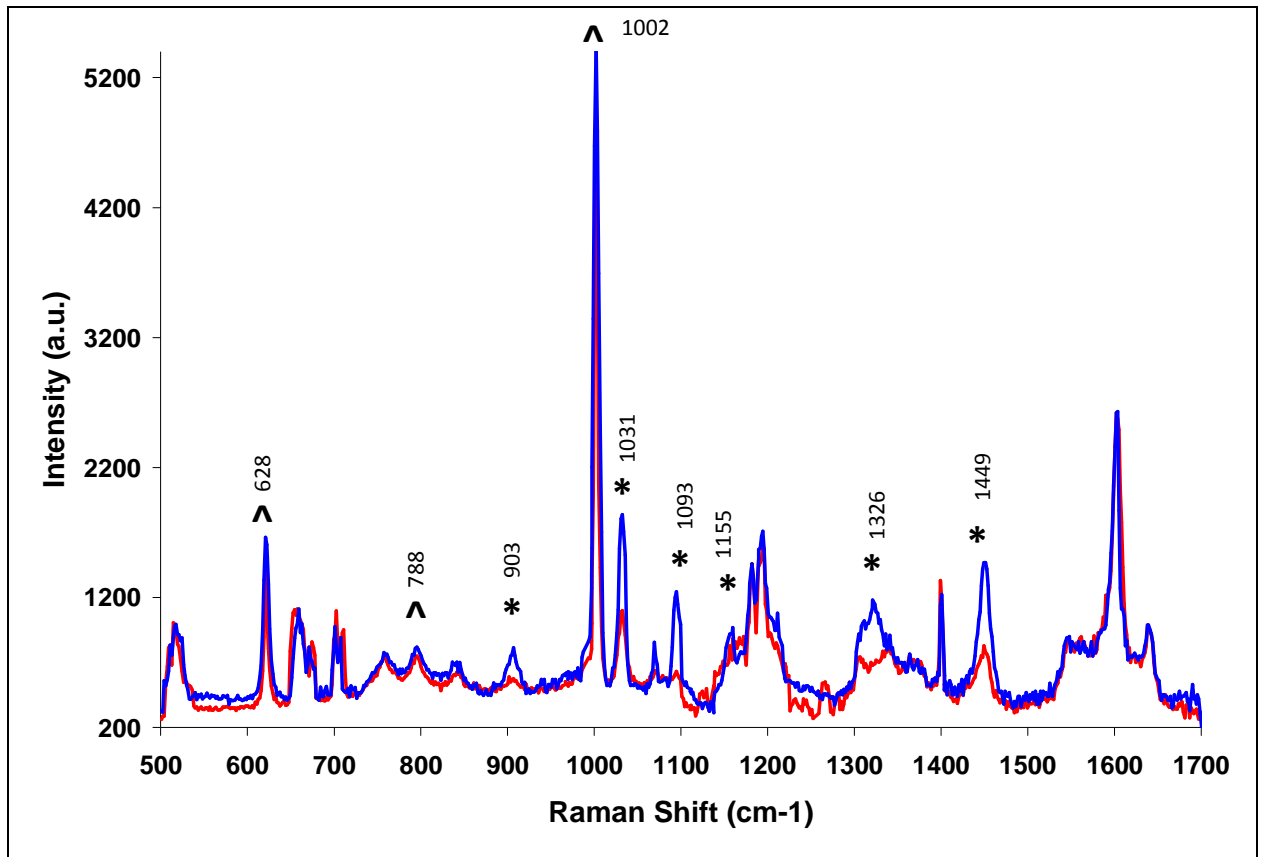
Figure 20. Superimposed mean Raman spectra from CD3/CD28-activated (red) and alloreactive T lymphocytes annotated with (*) foci of significant differences and (^) markers of cellular viability [5].
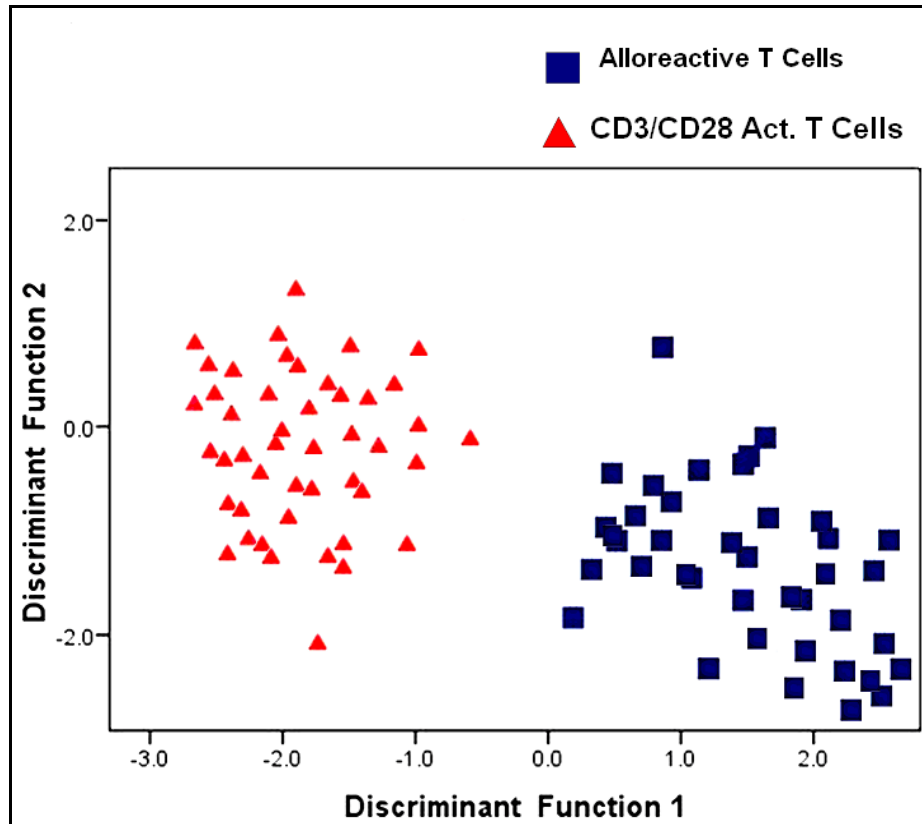
**Figure 21.** Discriminate function analysis of alloreactive versus CD3/CD28-activated T lymphocytes.

Table I. Comparative summary of relevant Raman shifts of CD3/CD28-activated, inactivated, alloreactive, and resting T lymphocytes. (See Abbreviation key below Table)

PA (cm^{-1})	PM of NSA (75) vs. Inact (75);%Δ; P Value	PM of NSA (75) vs. Rest (75); %Δ; P Value	PM of NSA (46) vs. Allo (40); %Δ; P Value	PM of Allo (40) vs. Inact (75); %Δ; P Value	PM of Allo (40) vs. Rest (75); %Δ; P Value	PM of Rest (75) vs. Inact (75); %Δ; P Value
628	1663.24 vs. 1684.01; NA; 0.7	1663.24 vs. 1652.33; NA; 0.9	1663.24 vs. 1602.52; NA; 0.3	1602.52 vs. 1684.01; NA; 0.12	1602.52 vs. 1652.33; NA; 0.6	1652.33 vs. 1684.01; NA; 0.89
788	805.86 vs. 818.95; NA; 0.91	805.86 vs. 807.50; NA; 0.72	805.86 vs. 809.2; NA; 0.62	808.1 vs. 818.95; NA; 0.75	808.12 vs. 807.50; NA; 0.9	807.50 vs. 818.95; NA; 0.88
903	736.7 vs. 828.92; ↑ 12.5%; 0.004	736.7 vs. 819.62; ↑ 11%; 0.007	736.7 vs. 814.89; ↑ 10%; 0.01	814.89 vs. 828.9; NA; 0.4	814.89 vs. 819.62; NA; 0.09	819.62 vs. 828.92; NA; 0.09
1002	5279.08 vs. 5438.8; NA; 0.82	5279.08 vs. 5520.1; NA; 0.8	5279.08 vs. 5490.2; NA; 0.78	5490.2 vs. 5438.8; NA; 0.91	5490.24 vs. 5520.1; NA; 0.8	5520.1 vs. 5438.8; NA; 0.76
1031	1390.8 vs. 1837.18; ↑ 32%; 0.002	1390.8 vs. 1815.92; ↑ 31%; 0.005	1390.8 vs. 1805.56; ↑ 29.8%; 0.003	1805.5 vs. 1837.1; NA; 0.62	1805.5 vs. 1815.92; NA; 0.09	1815.92 vs. 1837.1; NA; 0.4

Table I (cont). Comparative summary of relevant Raman shifts of CD3/CD28-activated, inactivated, alloreactive, and resting T lymphocytes.

PA (cm⁻¹)	PM of NSA (75) vs. Inact(75); %Δ; P Value	PM of NSA (75) vs. Rest (75); %Δ; P Value	PM of NSA (46) vs. Allo (40); %Δ; P Value	PM of Allo (40) vs. Inact (75); %Δ; P Value	PM of Allo (40) vs. Rest (75); %Δ; P Value	PM of Rest (75) vs. Inact (75); %Δ; P Value
1069	980.32 vs. 1024.0; ↑ 4.3%; 0.02	980.32 vs. 1012.8; ↑ 3.3%; 0.05	980.32 vs. 1021.7; NA; 0.4	1021.7 vs. 1024.0; NA; 0.1	1021.73 vs. 1012.8; NA; 0.1	1012.83 vs. 1024.0; NA; 0.65
1093	947.52 vs. 1245.08; ↑ 32%; 0.006	947.52 vs. 1199.85; ↑ 27%; 0.004	947.52 vs. 1145.08; ↑ 31%; 0.04	1145.0 vs. 1245.0; NA; 0.09	1145.08 vs. 1199.8; NA; 0.08	1199.85 vs. 1245.0; NA; 0.09
1155	1463.5 vs. 1914.44; ↑ 31%; 0.005	1463.5 vs. 1938.60; ↑ 32%; 0.009	1463.5 vs. 1924.44; ↑ 31%; 0.03	1924.4 vs. 1914.4; NA; 0.8	1924.4 vs. 1938.60; NA; 0.3	1938.60 vs. 1914.4; NA; 0.1
1182: 1195*	Ratio: 0.91 vs. 1.2; p = 0.006	Ratio: 0.91 vs. 1.05; p = 0.009	Ratio: 0.97 vs. 0.86; p = 0.8	Ratio: 0.86 vs. 1.2; p = 0.007	Ratio: 0.86 vs. 1.05; p = 0.002	Ratio: 1.05 vs. 1.2; p = 0.09
1326	1301.2 vs. 1600.26; ↑ 23%; 0.03	1301.20 vs. 1572.34; ↑ 21%; 0.02	1301.2 vs. 1608.3; ↑ 22.9%; 0.04	1608.3 vs. 1600.2; NA; 0.21	1608.3 vs. 1572.34; NA; 0.12	1572.34 vs. 1600.2; NA; 0.77
1449	1542.33 vs. 1834.9; ↑ 19 %; 0.001	1542.33 vs. 1833.02; ↑ 18.9; 0.002	1542.3 vs. 1832.92; ↑ 19%; 0.001	1832.9 vs. 1834.9; NA; 0.08	1832.92 vs. 1833.0; NA; 0.09	1833.0 vs. 1834.94; NA; 0.08

Data for **Table I** derived from averaged peak values of CD3/CD28, Inactivated, Alloreactive, and resting T cell samples at specified peak assignment. Values noted in ( ) correspond to number of T cells evaluated in each comparison. **Abbreviations:** PA- peak assignment; NSA- nonspecific antigen (CD3/CD28); Inact- inactivated T cells; Rest- resting T cells; Allo- alloreactive T cells; PM- peak magnitude; %Δ - percent change in peak magnitude; NA- peak magnitude change not significant; * Data corresponds to ratio of 1182 to 1195 peaks.

Chapter 6.4- Discussion

Raman shifts occurring at 903 cm^{-1}, 1031 cm^{-1}, 1093 cm^{-1}, 1155 cm^{-1}, 1326 cm^{-1}, and 1449 cm^{-1} were observed in the CD3/CD28-activated but not in the alloantigen-activated T cell samples. These foci of peak differences likely represent a specific conformational change in cell surface molecules reflecting a response to the particular CD3/CD28 (non-MHC restricted) stimulus. The greater number of foci of peak differences is related to the non-specific binding of the beads to the TCR which results in maximum stimulation free of anergy. When cross referencing these foci with established peak assignment data, they represent changes in nucleic acids (903 cm^{-1}, 1093 cm^{-1}, and 1449 cm^{-1}), amino acids (1031 cm^{-1}, and 1155 cm^{-1}), or both (1326 cm^{-1})- changes which are consistent with molecular processes responsible for the transcription, translation, and expression of cell surface receptors [20-23] (**Appendix B**). When further analyzing these peak differences that were unique to the CD3/CD28-activated T cells, there was a reduction in peak magnitudes observed in all six of the aforementioned peak positions. This is most likely represents a reshuffling rather than an absolute down-regulation of cell surface biomolecular material resulting from conformational changes in receptors, a concept that will be further explored in **Chapter 8**.

REFERENCES

1. Brown KL, Palyvoda OY, Thakur JS, Nehlsen-Cannarella SL, Fagoaga OR, Gruber SA, Auner GW. 2009. Differentiation of Alloreactive versus CD3/CD28 stimulated T-lymphocytes Using Raman Spectroscopy: A greater specificity for noninvasive acute renal allograft rejection detection. Cytometry A 75: p. 917-23.

2. Melamed, M.R., Mullaney, P.F., and Mendelsohn, M.L. 1990. Flow Cytometry and Sorting, 2nd ed. New York. Wiley-Liss.

3. Fleisher TA, Marti GE, Hagengruber C. 1988. Two-color flow cytometric analysis of monocyte depleted human blood lymphocyte subsets. Cytometry 9. p. 309-315.

4. Schwarting, R., Biedobitek, G., Stein, H. 1989. Cluster report: CD69. In: Knapp W, Dörken B, Gilks WR, et al, eds. Leucocyte Typing IV: White Cell Differentiation Antigens. New York, NY: Oxford University Press: p. 428-432.

5. Notingher I, Verrier S, Haque S, Polak JM, Hench LL. 2003. Spectroscopic study of human lung epithelial cells (A549) in culture: living cells versus dead cells. Biopolymers 72(4): p. 230-240.

CHAPTER 7- BIOMOLECULAR MODELING OF T LYMPHOCYTE ACTIVATION USING RAMAN SPECTROSCOPY

Chapter 7.1- Introduction

Based on data presented in **chapters 5** and **6**, which dealt with sensitivity and specificity, respectively, RS can detect key signature differences between activated and non-activated T lymphocytes and T lymphocytes that have been activated through different processes. However, one of the challenges of using RS in the larger biological narrative is linking spectral changes with biological processes that are known to be occurring and that have been verified through other independent methodologies. One of these independent methodologies involves using monoclonal antibodies (mAbs) to analyze the kinetics of cell surface receptor expression. This concept of kinetics suggests that T lymphocyte activation is defined not only by the characteristic up-regulation and conformational changes in specific cell surface receptors, but activation is also dependent on the differential *timing* of receptor expression.

There are certain specific receptors that are of interest when quantifying T cell activation. CD69 is a transient activation marker that is expressed as early as 2 hours after activation and is subsequently down-regulated by 55 hours post-activation [1-4]. Unlike CD69, receptors CD25 and CD71, and the Human Leukocyte Antigen DR (HLA DR) receptor follow a delayed expression pattern, appearing at 13, 25, and 48 hours following activation, respectively. These receptors remain at high levels throughout the activation/clonal expansion process. A summary of receptor expression kinetics is depicted in **Figure 22.** CD69 is a type II transmembrane homodimeric glycoprotein that is 22.5 kD in size [5]. CD25 is a 55 kD type I transmembrane glycoprotein also known as the low affinity IL-2 receptor α chain [6]. CD71, also known as the human transferrin receptor 1, is a homodimeric type II membrane glycoprotein responsible for

cellular iron uptake via receptor-mediated endocytosis while HLA DR is a heterodimer which serves as a ligand for the TCR [7]. The α and β subunits of the HLA DR receptor have two extracellular domains, a membrane spanning domain, and a cytoplasmic tail. HLA DR is central to the donor-recipient crossmatching process that minimizes the likelihood of organ rejection [8]. The study outlined in this chapter will focus on the kinetics of CD69, CD25, and CD71.

The goal of this study was to set up a parallel investigation of T lymphocyte activation using both differential mAb staining and RS. We hypothesized that during the course of activation, changes in the specific receptors expressed on the cell surface with subsequent changes in mAb staining patterns would be significant. We further hypothesize that by analyzing unstained representative lymphocytes at the same time points as the mAb staining, we will be able to correlate the biomolecular process of up-regulating a cell surface receptor in response to a stimulus with Raman shifts detected by RS.
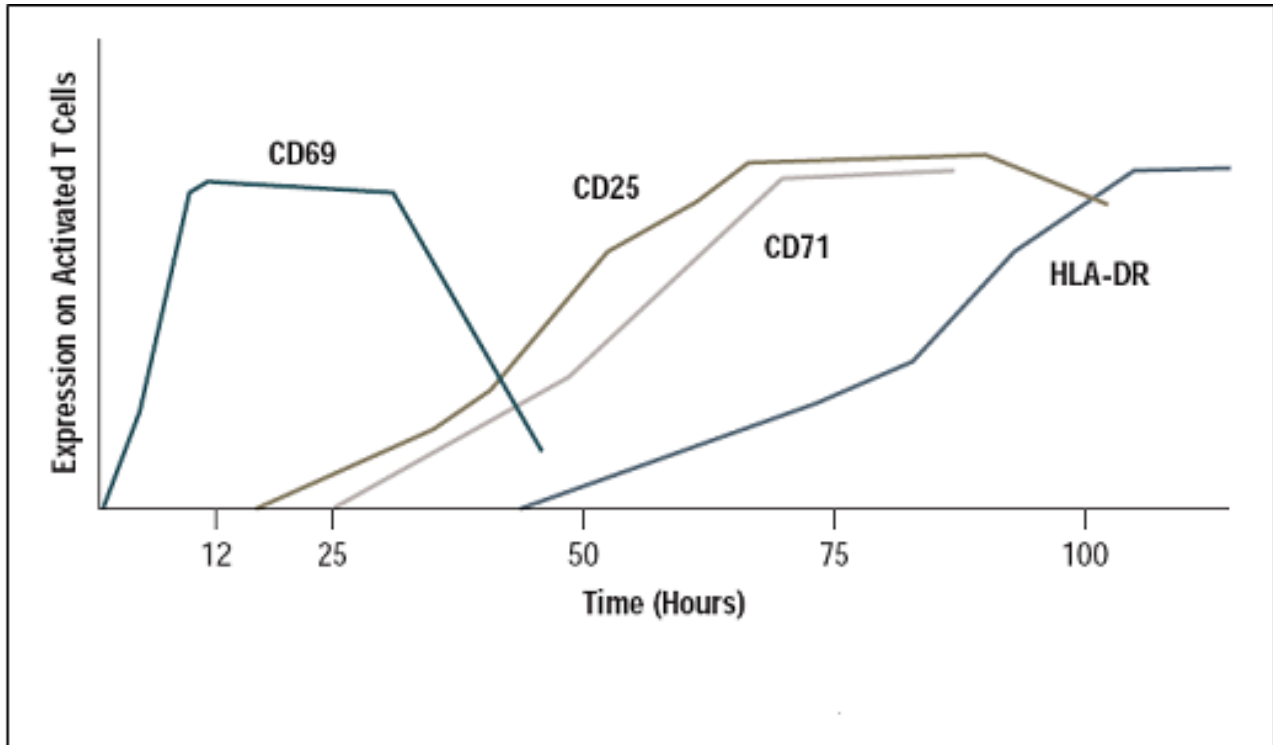
Figure 22. Kinetics of antigen expression [9].

Chapter 7.2- Materials and Methods

7.2.1 Cell Preparation and Mitogen Induction

Prior approval for the study was obtained from the Wayne State University HIC. Sodium-heparinized venous blood was collected from healthy participants and incubated with 40 µL of a 1:1 mixture of Concanavalin A (*Canavalia ensiformios* agarose; Sigma, St. Louis, MO) and pokeweed (*Phytolacca Americana* lectin; Sigma, St. Louis, MO). Following a 24-hour mitogen incubation period, T lymphocytes were isolated directly from the peripheral blood using a Dynal T cell negative isolation kit (Invitrogen, Canoga Park, CA) and resuspended in complete media. Activated T lymphocytes were confirmed and isolated using flow cytometry (**Appendix C**). This

purely activated (and antibody free) T cell population was then cultured at 37°C in 5% CO_2 in multi-well plates in complete media containing recombinant interleukin 2 (50U/ml; Becton Dickinson, San Jose, CA). Negative control samples were cultured in parallel and consisted of T lymphocytes pretreated with Mitomycin C (Sigma, St. Louis, MO; 0.025 mg of Mitomycin C (0.5 mg/ml) to each 1 ml of cell suspension) for 20 minutes. T lymphocyte cultures were continued for 72 hours with daily viability testing, daily RS analysis, and mAb staining at 48 and 72 hours.

7.2.2- Monoclonal Antibody Staining

Representative aliquots of mitogen-activated T lymphocytes were collected at 48 and 72 hours following initial stimulus and washed three times using PBS. All cells collected at each time period were stained with a 4',6-diaminidino-2-phenylindole (DAPI; Thermo Fisher Scientific, Rockford, IL) nuclear stain that was contained in an anti-fade solution. In addition, cells were divided into two groups at each time interval. The first group was treated with paraformaldehyde (Sigma, St. Louis, MO) and incubated overnight with the transient cell surface mAb, CD69 (Becton Dickinson, San Jose, CA). The second group was treated with permeabilizing solution (Becton Dickson, San Jose, CA) and incubated overnight with the intracellular antibody cocktail containing a CD25/CD71 (Becton Dickson, San Jose, CA) mixture with subsequent fixing with paraformaldehyde. Cells were viewed using a Nikon Eclipse TE 2000-U inverted microscope with images being captured and processed using Metavue 6.2r5 software (Downingtown, PA).

7.2.3 Raman Spectroscopic Analysis

Raman spectroscopic analysis was carried out daily on non-antibody bound lymphocytes. Spectra from the 48 and 72 hour time points were compared to mAb staining data derived from methods described previously. Prior to analysis, all samples were washed with PBS. Cells were allowed to settle within the analysis reservoir placed on a leveled microscope stage. Only rounded, non-adhered, isolated and individualized T lymphocytes were selected for study. Each sample was analyzed using an identical protocol and spectroscopic parameters. Using an enhanced video imaging system, T lymphocytes were aligned in the laser target area so that the focus point was centered on the lymphocyte. Images were captured before and after each measurement with no noted cell shifting or destruction observed. Wire 2 software (Renishaw plc, Old Town, United Kingdom) was utilized in conjunction with the Raman system for quantitative measurements. RS measurements were conducted using a Renishaw InVia 2000 microscope-spectrometer with a Leica 63X water immersion objective (NA= 1.20). T lymphocytes were analyzed using a 514.5 nm (green) Ar^+ excitation wavelength. Laser power was set at 50% (8-12 mW) for a 2-4 μm laser spot size. Spectra were collected in the backscattering geometry with a 10 second integration time over a range of 500 to 1700 cm^{-1}.   The spectral resolution was ~ 4 cm^{-1}.

7.2.4- Statistical Analysis

Prior to statistical analysis, all data were checked for various types of noise as described in **section 5.2.5**. Student's t-test was utilized to further quantify differences in peaks. The data were analyzed for the presence of various independent groups using DFA. Graphical and quantitative analysis of data was accomplished using SPSS version 15 software (Statistical Software, Chicago, IL).

Chapter 7.3- Results

Forty-eight hours following mitogen stimulation, representative T lymphocytes were stained for activation markers according to the procedures stated above. In addition, 50 T lymphocytes at this same time point were analyzed using RS. All lymphocytes included in this analysis were verified to be intact and non-apoptotic. In addition, DAPI staining revealed that cells analyzed were nucleus containing and viable (**Figure 23, Panel A** and **D**).

High expression of the transient CD69 cell surface receptor was evident when assessing qualitative antigen expression at 48 hours via mAb staining (**Figure 23, Panel B**). However, T lymphocytes at the 72 hour time point showed no appreciable binding of the fluorescent tag (**Figure 23, Panel E**.). Moreover, 48 hour RS- analyzed T lymphocytes demonstrated a significant peak difference at the 1585 cm^{-1} position (**Figure 24**). The 48 hour samples had a mean peak magnitude of 2899.23 ± 165.38 compared with 2364.39 ± 229.62 for the 72 hour samples. For the 48 hour samples, this represented a 22% (p = 0.01) increase in peak magnitude at this position.

There was a precipitous increase in the expression of CD25/CD71 from 48 to 72 hours (**Figure 23, Panels C** and **F**). In addition, the corresponding RS-analysis demonstrated two significant peak differences at the 903 cm^{-1} and 1449 cm^{-1} positions (**Figure 25**). There was an 18% (p = 0.04) and 11% (p = 0.001) increase in peak magnitudes at the 903 cm^{-1} and 1449 cm^{-1}, respectively.
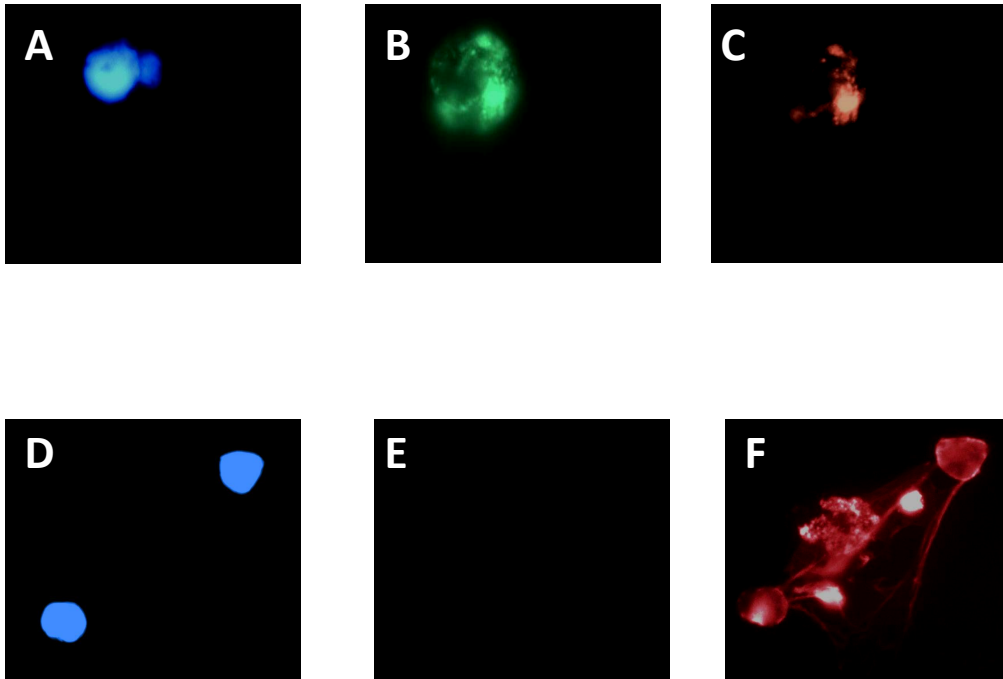
Figure 23. Representative 48 hour (Panels A-C) and 72 hour (Panels D-F) antibody stained mitogen activated T lymphocytes. Panels A and D- DAPI stain. Panels B and E- CD69 stain (FITC).

Panels C and F- CD25/CD71 stain (PE).

Figure 24. Mean (n = 50) Raman spectral changes at 48 hours with accompanying antibody staining results for 48 hours and 72 hours- (insets A and B, respectively). Arrow indicates significant peak difference at 48 hours. Note: for additional peaks associated with activation please see **Figure 12A and 15A**.

Figure 25. Mean (n = 50) Raman spectral changes at 72 hours (red) with accompanying antibody staining results for 48 hours and 72 hours- (insets A and B, respectively). Arr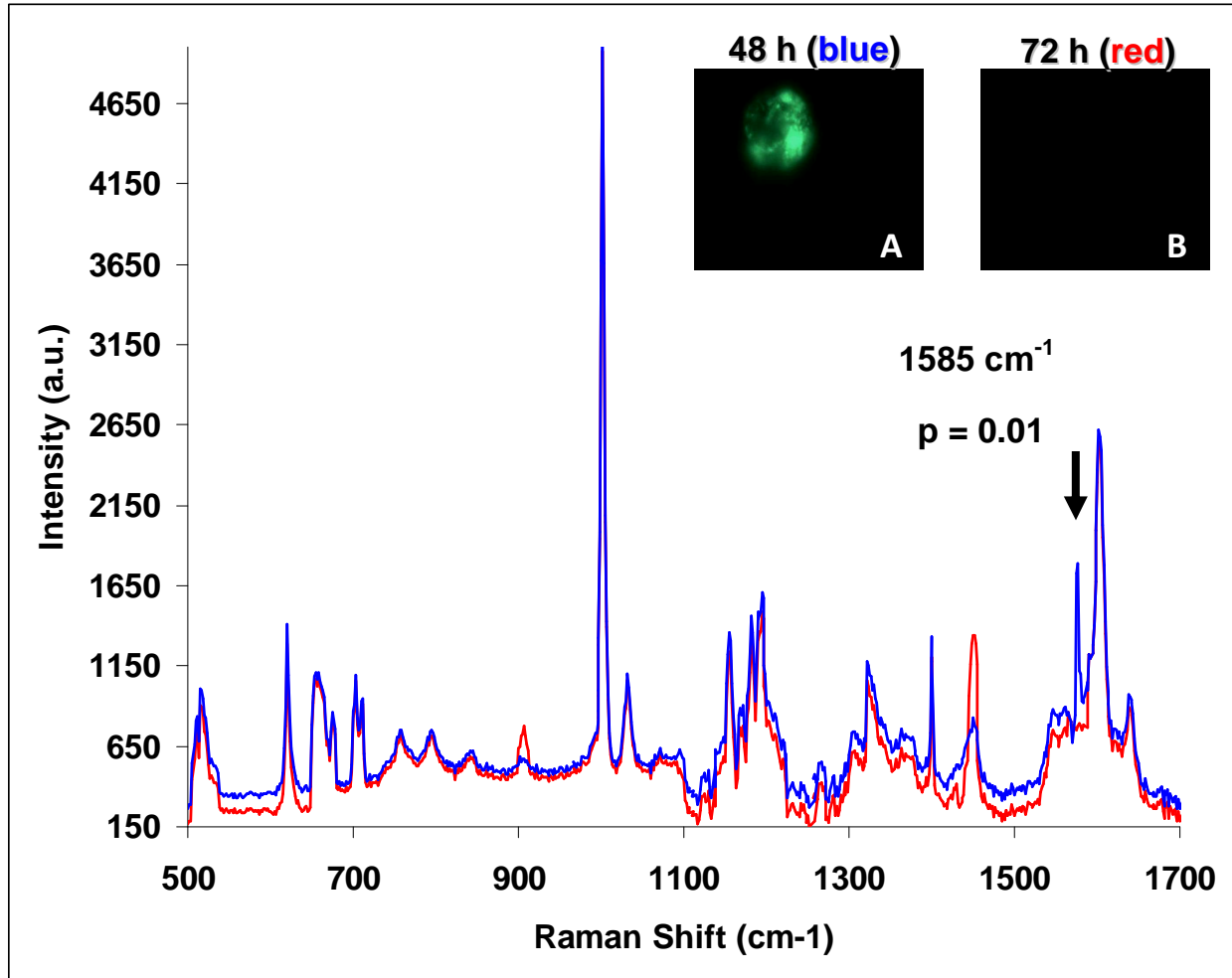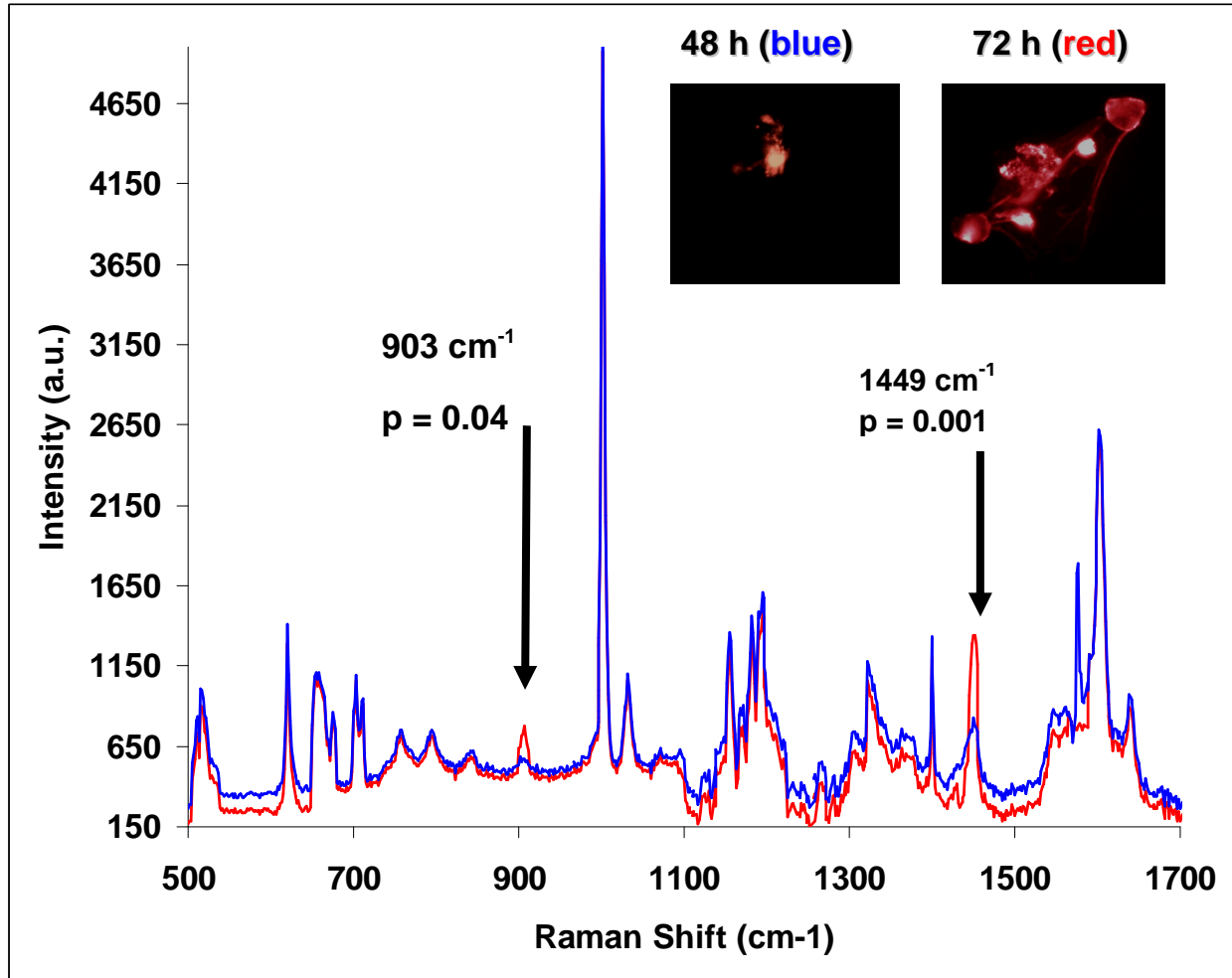ows indicate significant peak changes at 72 hours. Note: for additional peaks associated with activation please see **Figure 12A and 15A**.

Chapter 7.4- Discussion

The goal of this study was to link RS spectral changes with a direct method of measuring the biomolecular process of cell surface receptor up-regulation and expression. At 48 hours, the T lymphocyte is considered to be in the "early" phase of activation [10].   This early activation resulted in transient CD69 expression detected by mAb staining panels. This was coupled with RS signature changes at the 1585 cm^{-1} position, consistent with carbohydrate (C-O-C deformation) and nucleic acid (Guanine, Adenine) turnover [11] (**Appendix B**). Conversely, "late" T lymphocyte activation was dominated by the up-regulation of CD25 and CD71 [10]. The expression of CD25 and CD71 was marked by a significant qualitative increase in the intensity of the fluorescent tag which was matched by RS signature changes at the 903 cm^{-1} and 1449 cm^{-1} peak positions. These Raman shifts were consistent with conformational changes in protein (C-C backbone stretching, α helix changes), carbohydrate (CH deformation), and lipid (CH_2 bending) molecular events [11] (**Appendix B**). The specific ramifications of the C-O-C deformation at 48 hours and the C-C backbone stretching and alpha helix changes at 72 hours will be further discussed on **Chapter 8**.

This foundational study looked at the molecular events following activation by a mitogen (i.e. super-antigen). By tracking the up- and down-regulation of receptors through mAb binding which is dictated by Fab domain specificity, we were able to mark conformational changes in the cell surface topography. We were then able to couple these conformational changes with Raman shifts that occur within the same time frame. The next chapter will explore how alterations in 3D structure can affect Raman scattering.

REFERENCES

1. Simms P and Ellis T. 1996. Utility of Flow Cytometric Detection of CD69 Expression as a Rapid Method for Determining Poly- and Oligoclonal Lymphocyte Activation. Clinical and Diagnostic Laboratory Immunology 3(3). p. 301–304.

2. Posselt A, Vincenti F, Bedolli M, Lantz M, Roberts J, Hirose R. 2003. CD69 expression on peripheral CD8 T cells correlates with acute rejection in renal transplant recipients. Transplantation 76(1). p. 190-195.

3. Mardiney M, Brown M, Fleisher T. 1996. Measurement of T-cell CD69 expression: A rapid and efficient means to assess mitogen- or antigen-induced proliferative capacity in normals. Cytometry 26(4). p. 305-310.

4. Alonso-Camino V, Sánchez-Martín D, Compte M, Sanz L, Alvarez-Vallina L. 2009. Lymphocyte display: a novel antibody selection platform based on T cell activation. PLoS One 24;4(9): p. e7174.

5. Cebrian M,Yague E,Rincon M,Lopez-Botet M,de Landazuri MO,Sanchez-Madrid F Triggering of T cell proliferation through AIM, an activation inducer molecule expressed on activated human lymphocytes. J Exp Med 1988 168:1621

6. Taniguchi T, Minami Y. 1993. The IL-2/IL-2 receptor system: a current overview. Cell 73(1). p. 5-8.

7. Antonaci S, Tortorella C, Polignano A, Ottolenghi A, Jirillo E, and Bonomo L. 1991. Modulating Effects on CD25 and CD71 Antigen Expression by Lectin-Stimulated T

Lymphocytes in the Elderly. Immunopharmacology and Immunotoxicology 13;1-2; p. 87-100.

8. Marsh SG, Albert ED, Bodmer WF, Bontrop RE, Dupont B, Erlich HA, Geraghty DE, Hansen JA, Hurley CK, Mach B, Mayr WR, Parham P, Petersdorf EW, Sasazuki T, Schreuder GM, Strominger JL, Svejgaard A, Terasaki PI, and Trowsdale J. 2005. Nomenclature for factors of the HLA System, 2004. Tissue antigens 65: p. 301–369.

9. Maino V, et al. FastImmune Assay System. A rapid and comprehensive system for assessing lymphocyte function by flow cytometry. Supplemental.

10. Janeway C, Travers P, Walport M, Capra J. 1999. T Cell Mediated Immunity. In: Austin, P., Lawrence, E. Immunobiology: The immune system in health and disease 4th edition. Garland Publishing, NY p. 510-514.

11. Notingher I. 2007. Raman Spectroscopy. Cell-based Biosensors. Sensors *7*, p. 1343-1358.

CHAPTER 8- CONCLUSION AND FUTURE DIRECTIONS

Chapter 8.1- Conclusion

The immune system reflects a duality of requirements dictated by the need to remain relatively conserved in many of its activation pathways, while maintaining a high level of specificity for a particular antigen. This notion has been thoroughly demonstrated through studies involving the MHC, TCR, and other cell surface receptors involved in the activation process [1]. Our series of studies suggest that when examining the array of receptors expressed during varying methods of activation using the RS system, a duality of conservation and specificity is articulated via unique Raman spectroscopic shifts. When analyzing the ratios of the 1182:1195 cm^{-1} peaks, we found a similar shift in the alloreactive, CD3/CD28-activated, and mitogen-activated samples. However, these shifts were not present in the inactivated or resting T lymphocyte populations. This shift likely represents a change in light scattering that is a result of a conformational change in the CD3-TCR 3D structure and/or adjacent membrane, which is necessary for all forms of activation regardless of the initial stimulus. To further explore the link between conformational changes in 3D structure and characteristic Raman shifts observed in our study, let us consider the structural immunology work carried out by Lee and colleagues [2] who reported on the specific TCR residue changes responsible for driving alterations in 3D structure. The authors compared the contributions of residues involved in the binding of the TCR to self- versus allo-MHC molecules. They found that the self- and allo-MHC binding residues differed at 25 of the 41 positions within the CDR2 and CDR3 regions of the variable α and β domains. Of these two regions, the CDR3 had the greatest influence on binding differences which was attributed to the increased mobility of the CDR3 containing loop [2]. These residues were further categorized based on whether they were significantly, intermediately, or non-significantly

involved in binding (**Figure 26).** This study illustrates the key principle that even individual residue differences in the binding domain of the TCR can convey significant changes in binding specificity, which is ultimately manifested as changes in receptor form.
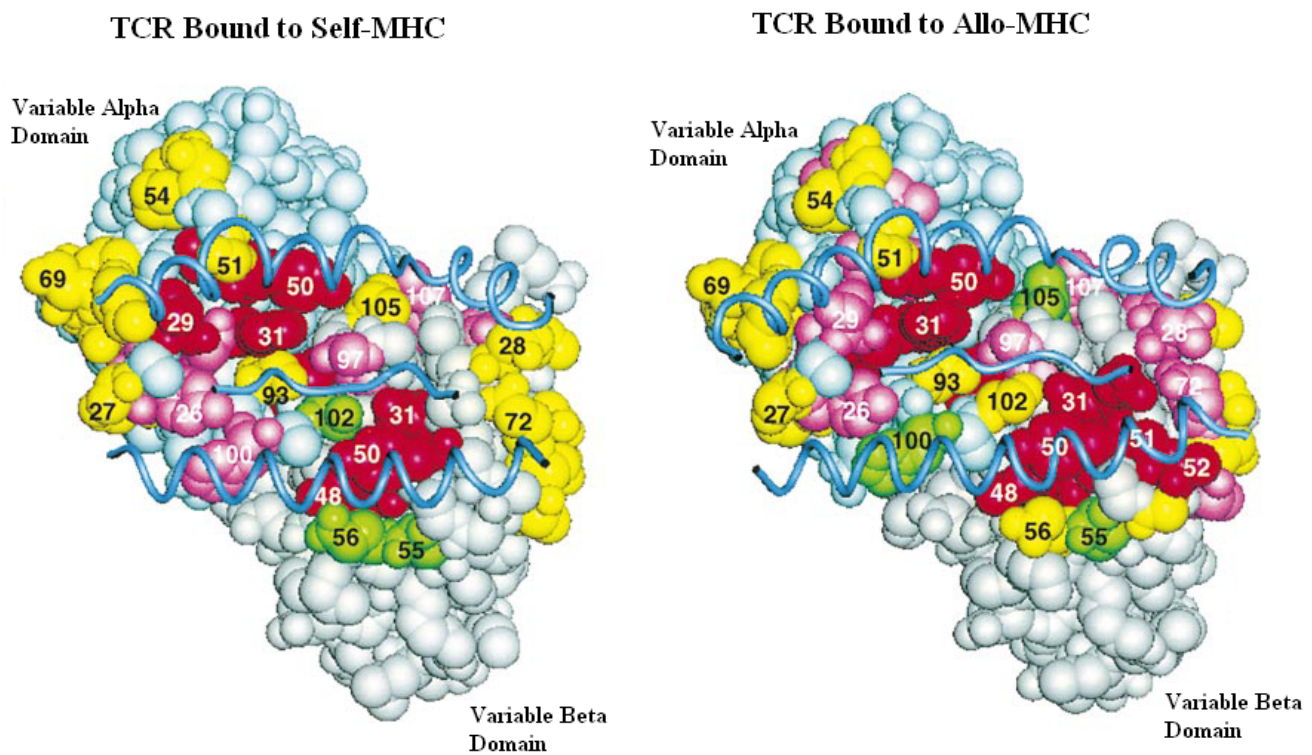
Figure 26. Differences in 3D confirmation and receptor structure dictate whether the TCR will bind to self- versus allo-MHC molecules. Residues in red indicate those with the greatest effect on binding; Pink residues have intermediate effect on binding; Yellow residues have negligible effect of binding. Blue lines represent the binding orientation of antigen peptide (curved line) and two domains of the MHC (coiled lines). Note the differences in distribution and number assignments of the red residues [2].

In addition to factors influencing TCR form, the authors dealt with function. They showed that T lymphocyte activity was reduced by upwards to 90% when single site mutations were introduced at eight amino acid residues in the variable alpha and beta domains. This observation aptly demonstrates that subtle changes in amino acid residues in the exposed portion of the TCR can dramatically affect function. When these aforementioned concepts of form and function are juxtaposed and placed in the context of our study which analyzed the conformational changes in, and variations of, the 3D structure of the TCR using RS, we find a link between the structural Immunobiology and changes in Raman scattering (**Figure 27**). Published peak assignments [3-6] for the 1182:1195 cm^{-1} position, which were shared by all activated T lymphocytes, suggests that the observed shifts represent changes in tyrosine and phenylalanine, two amino acids that are important in the dimerization of the TCR- CD3 complex via phosphorylation by Zap-70. They may also represent residues within the prominent binding domain of the TCR that were exposed by conformational changes in the aforementioned CDRs of the α and β chains [7] .

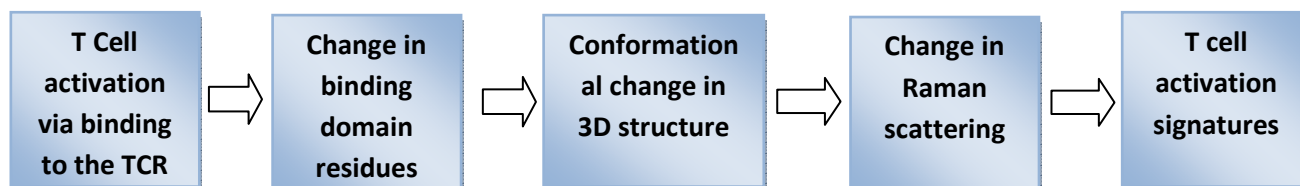| T Cell activation via binding to the TCR | | Change in binding domain residues | | Conformational change in 3D structure | | Change in Raman scattering | | T cell activation signatures |

Figure 27. Proposed structural etiology for observed Raman shifts and subsequent activation signature differences.

The Raman shift at the 1182:1195 cm^{-1} position, which was shared by all activated T lymphocytes, can be contrasted with shifts occurring at 903 cm^{-1}, 1093 cm^{-1}, and 1449 cm^{-1}, that were specific to CD3/CD28 and mitogen-activated lymphocytes, but not the alloreactive T lymphocyte population. Moreover, signature differences at positions 1031 cm^{-1}, 1155 cm^{-1}, and 1326 cm^{-1} were specific only to CD3/CD28-activated lymphocytes, while position 1585 cm^{-1} was unique only to the mitogen-activated samples. These differences can be explained by the scattering changes that occur as a result of de novo up-regulation of CD25, CD69, and CD71. These structures dramatically change the topography of the cell surface and thus significantly alter the way that light scattering occurs and because the specific 3D structure of the particular receptor expressed is unique to that receptor, it leads to a unique spectral shift that contributes to the entire activation signature. By coupling published peak assignment data [3-6] with shifts noted in each of the activated T lymphocyte groups, we observed that CD3/CD28 and mitogen activated T lymphocytes underwent C-C backbone, alpha helix, and C-H deformation changes in protein structures. Due to the mixed contribution that the CD25 and CD71 receptors provide to light scattering and their similar expression patterns (i.e. timing and type of stimulus triggering their expression), separating and assigning individualized proteinaceous changes is difficult. However, in the case of the CD69 receptor, our expression kinetics data (**Chapter 7**) provides a method for this individualized assignment. The transient nature of CD69 expression also leads to a transient state of its Raman scattering contribution. Based on this observation, we can conclude that the CD69 receptor demonstrated a unique shift at 1585 cm^{-1} that resulted from C-double bond-C phenylalanine and tyrosine residue changes in its protein structure.

When the observed Raman shifts for all T lymphocyte groups are taken as a collective we find that there were significant changes in lipid, carbohydrate, protein, and nucleic acid groups

that defined differences between activated and non-activated T lymphocytes. The presence of this array of biomolecular materials involved in the process of activation can be clearly accounted for by the requirements and results of DNA transcription, translation, processing of cell surface receptors in the rough endoplasmic reticulum and Golgi apparatus, delivery and membrane docking of lipid-lined vesicles containing refined receptors, and expression of these carbohydrate-covered receptors on the cell surface. However, from a spectroscopic point of view, it would be expected that if our RS analysis was confined solely to the external surface of the cell, there would be shifts that encompassed all categories except nucleic acids, for this content does not exist outside of the intracellular nucleus/ribosome context. The presence of these shifts involving nuclear material seen at different positions in all forms of activated T lymphocytes can be attributed to the resolution and penetration depth of the laser used in our analysis. The diameter of a T lymphocyte is ~ 10-12 μm while the laser spot size used in our experiments was ~ 3 μm. Although this spot size allowed for accurate analysis of the T lymphocyte, the shape and proportional dimensions of laser diameter to cell diameter yielded a resulting spectrum that was a composite of Raman shifts from receptor groups (carbohydrates and proteins), adjacent membrane (lipids), and sub-membranous regions (nucleic acids) (**Figure 28**). This mixed contribution is the basis of our activation signatures.
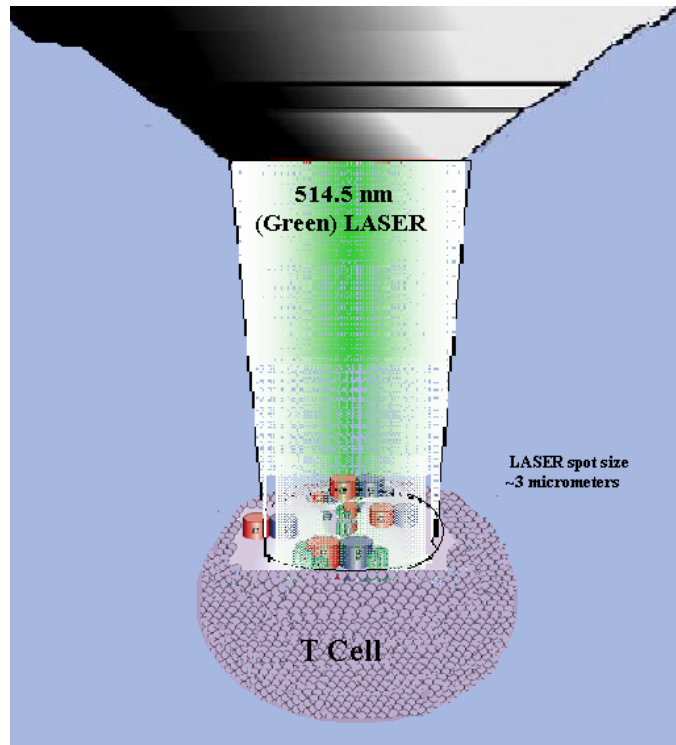
Figure 28. Laser sampling area of T lymphocyte surface and subsurface that includes multiple receptor groups, proteins, and lipids.

RS-based activation signatures reflect the biomolecular diversity resulting from the particular form of stimulation and are the basis of how a RS system could detect activated lymphocytes with high sensitivity and specificity. The value of this high sensitivity and specificity is two-fold. First, it provides an avenue to transition away from the paradigm of using invasive biopsies to confirm the diagnosis of AR and also provides an alternative to protocol biopsies to detect SCAR. Second, RS detection of AR offers a modality that could significantly reduce the delay in AR diagnosis. Under the current diagnostic algorithm, delays in treatment are created due to the need to eliminate other potential causes of serum creatinine elevations, thus

potentially allowing further histologic damage to the nephrons of transplanted grafts that continue to be in limited supply.

The overall conclusion of this dissertation is that with further refinement, RS can serve as a technological tool capable of detecting activated T lymphocytes (sensitivity) in urine or blood while offering additional information as to the particular method of nonspecific or MHC-restricted activation (specificity) based on the biomolecular and structural modeling of cell surface receptors.

Chapter 8.2- Future Directions

To gain further information concerning the biomolecular process that occurs during all stages of T lymphocyte activation, multi-spectral RS could be utilized in conjunction with a live cell imager, a device designed to allow for enclosed cell culturing and continuous RS analysis. This experimental design could effectively track Raman shifts from the very early steps of DNA transcription to the maturation of cell surface receptors and clonal expansion. This system could be enhanced with use of atomic force microscopy (AFM), a device that passes an ultrasensitive lever (cantilever) over a measured substance. The cantilever is designed to deflect according to surface patterning of the measured substance and thus provide precise topographic data. AFM has a resolution of < 1nm and can directly quantify the conformational change in a single receptor thereby allowing data collection regarding the evolution of individual receptors in response to an activation stimulus [8-10]. This high resolution can provide an alternative approach to the comprehensive analysis (receptor, adjacent membrane, and sub-membranous region) that a 4 µm laser spot size currently provides.

The potential applications of RS-based T lymphocyte analysis in the medical arena are vast. One such application could be the development of a comprehensive panel of clinically relevant signatures based upon viral (CMV and BK virus), fungal (Candida), and bacterial (E. coli) stimuli. These pathogens have a particularly devastating effect on graft survival in the transplant population. A rapid, accurate, noninvasive test for these pathogens (and others) would prove invaluable in the treatment of infectious diseases.

Another application involves using RS as a functional T cell assay. Based upon the notion that the true metric of adequate immunosuppressive therapy is the *functional* suppression of T lymphocyte activation measured at the level of the T cell, the RS system could be used to titrate immunosuppressant levels in an individualized way. Currently, dosing of powerful and sometimes toxic immunosuppressant medication is based on semi-standardized drug target levels, which often are limited by inter- and intra-patient variability and side-effect tolerance. RS could be used to rapidly assess the real-time immunologic temperament of T cells based on their activation state within the guise of the individual patient's current medication regimen. This would allow clinicians to decrease dosages to levels that are functionally adequate for each particular patient and thus avoid unwanted dose-related side effects while substantially reducing costs.

In addition to transplant immunology and infectious disease, T lymphocyte activation plays a pivotal role in oncology. Whether it is melanoma, hematologic cancers, or the various solid organ, connective or soft tissue malignancies, T cell changes may provide one of the earliest clues to the presence of these disease states. RS analysis of an appropriate oncological model could add to the growing body of knowledge concerning biomarkers directed at early cancer detection.

This dissertation outlines the use of RS in the resolution and modeling of cell surface receptor differences that define T lymphocyte activation. The accurate detection of T lymphocyte activation within a biomatrix is the foundational step toward the development of a noninvasive tool capable of accurately detecting AR in real-time within the clinical setting.
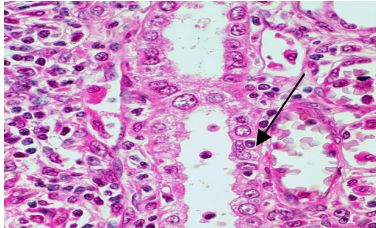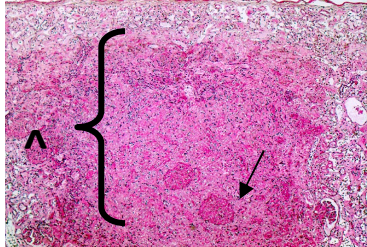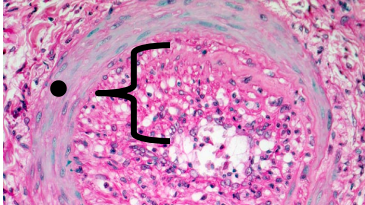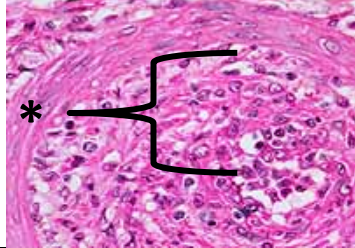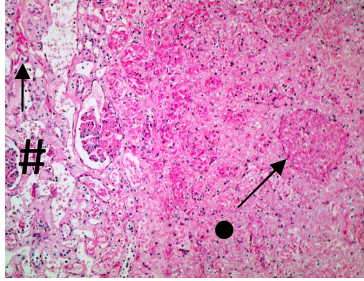
REFERENCES

1. Janeway C, Travers P, Walport M, Capra J. 1999. The major histocompatibility complex of genes: organization and polymorphism, In: Austin, P., Lawrence, E. eds., Immunobiology: The immune system in health and disease, 4th edition. Garland Publishing, NY. p. 135, 148.

2. Lee PU, Churchill HR, Daniels M, Jameson SC, Kranz DM. Role of 2CT cell receptor residues in the binding of self- and allo-major histocompatibility complexes. J Exp Med. 2000 Apr 17;191(8):1355-64.

3. Deng H, Bloomfield V, Benevides J, Thomas G. 1999. Dependence of the Raman signature of genomic B-DNA on nucleotide base sequence. Biopolymers 50, p. 656-666.

4. Erfurth S, Peticolas W. 1975. Melting and premelting phenomenon in DNA by laser Raman-scattering. Biopolymers 14, p. 247-264.

5. Benevides J, Thomas G. 1983. Characterization of DNA structures by Raman spectroscopy: high-salt and low-salt forms of double helical poly (dG-dC) in H2O and D2O solutions and application to B, Z and A-DNA. Nucleic Acids Res 11, p. 5747-5761.

6. Puppels G, Demul F, Otto C, Greve J, Robertnicoud M, Arndtjovin D, Jovin T. 1990. Studying single living cells and chromosomes by confocal Raman microspectroscopy. Nature 347, p. 301-303.

7. Signaling through immune system receptors. Immunobiology. NCBI Bookshelf. http://www.ncbi.nlm.nih.gov/bookshelf/br.fcgi?book=imm&part=A673. 1/2/2010.

8. Fotiadis, D., Hasler, L., Muller, D.J., Stahlberg, H., Kistler, J., and Engel, A. 2000. Surface tongue-and-groove contours on lens MIP facilitate cell-to-cell adherence. Journal of Molecular Biology 300, p. 779-789.

9. Reviakine, I., Bergsma-Schutter, W., and Brisson, A. 1998. Growth of protein 2-d crystals on supported planar lipid bilayers imaged in situ by AFM. Journal of Structural Biology 121, 356-362.

10. Muller, D.J., and Engel, A. 1999. Voltage and pH-induced channel closure of porin OmpF visualized by atomic force microscopy. Journal of Molecular Biology 285, p. 1347-1351.

APPENDICES

Appendix A. Banff 97 Criteria and Histologic Phenotype [1, 2]

| Grade	Pathological Description	Histology
IA	Tubulointerstitial infiltrates >25% of parenchyma with foci of moderate tubulitis (arrow)	
IB	Significant interstitial infiltration (^) with foci of severe tubulitis (arrow)	
IIA	Mild to moderate intimal arteritis	
IIB	Severe intimal arteritis comprising the luminal area- nearly complete occlusion (*)	
III	Transmural arteritis and/or dilated vessels (#) with arterial fibrinoid change and necrosis of medial smooth muscle cells (•)	

Appendix B- Raman Spectroscopic Peak Assignments [3-5]

| Peak (cm^{-1})	Assignment
618-621	Protein: C-C twist phenylalanine
640-645	Protein: C5 stretch, C-C twist Tyr
666-667	Nucleic Acid: T,G, tyrosine, G backbone in RNA
717	Lipids: CN$^+$(CH$_3$)$_3$ stretch
725-729	Nucleic Acid: Adenine breathing
729	Nucleic Acid: Adenine
746	Nucleic Acid: Thymine breathing
760	Protein: Ring breath tryptophan
782	Nucleic Acid: uracil, cytosine, thymine ring breathing
788	Nucleic Acid: O-P-O stretching, uracil
903-937	Protein: C-C backbone stretching α -helix; Carbohydrates: C-O-C glycos. Nucleic Acid O-P-O asym. stretch
1002-1005	Protein: Sym. Ring breathing phenylalanine
1031-1033	Protein: C-N stretching, C-H in-plane phenylalanine

1053	Protein: C-N stretching, C-O stretching
1069-1095	Nucleic Acid: phosphate stretching; Lipids: chain C-C stretching; Carbohydrates: C-O, C-C stretching
1126-1128	Protein: C-N stretching
1155-1158	Protein: C-C, C-N stretching
1175	Protein: C-H bending tyrosine
1182-1195	Protein: C-H bending, amide III, tyrosine, phenylalanine; Nucleic Acid: adenine, thymine
1208	Nucleic Acid: adenine, thymine; Protein: Amide III
1319-1326	Nucleic Acid: guanine; Protein: C-H deformation
1342	Nucleic Acid: adenine, guanine; Protein: C-H; Carbohydrates: C-H deformation
1420-1480	Nucleic Acid: guanine, adenine, C-H deformation; Protein: C-H; Lipids: C-H deformation; Carbohydrates: C-H deformation
1578-1585	Nucleic Acid: guanine, adenine. Protein: C-double bond-C phenylalanine, tyrosine
1607	Protein: C-double bond-C phenylalanine, tyrosine
1655-1680	Protein: Amide I; Lipids: C-double bond-C stretching

Appendix C. Flow Cytometry Directed Verification of T –lymphocyte Activation Status.
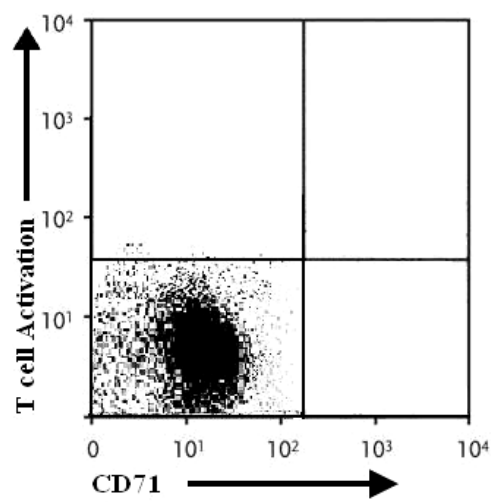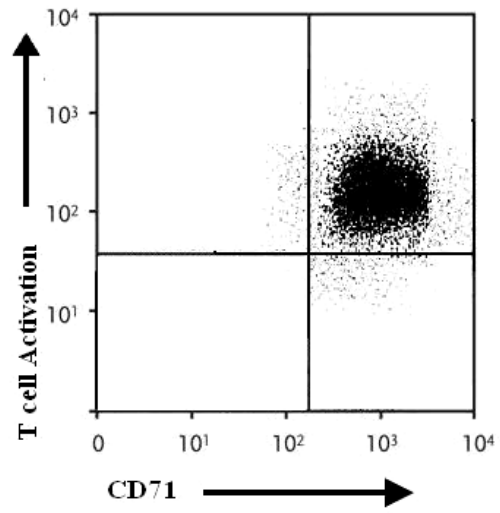

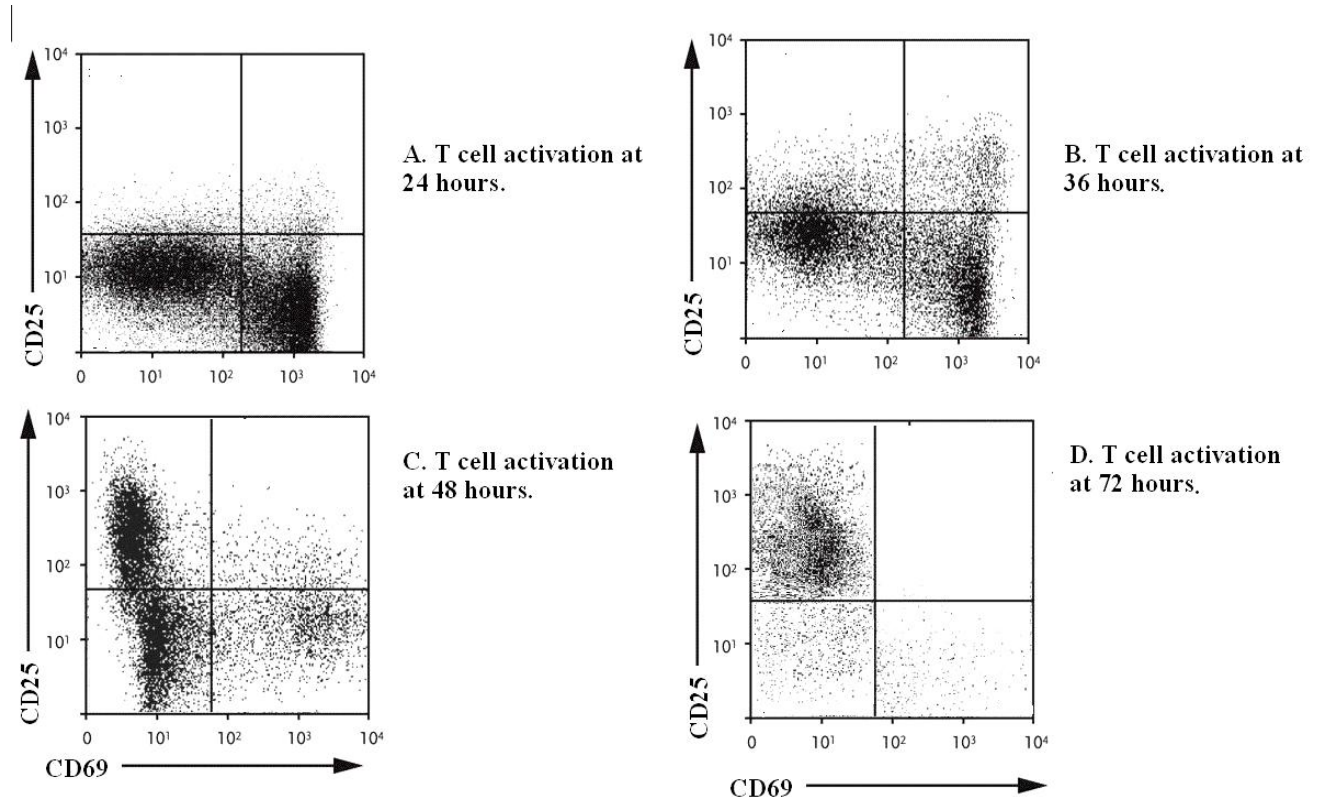A. Inactivated T lymphocytes
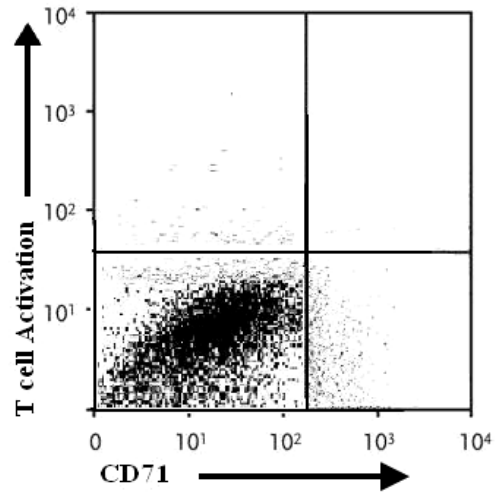
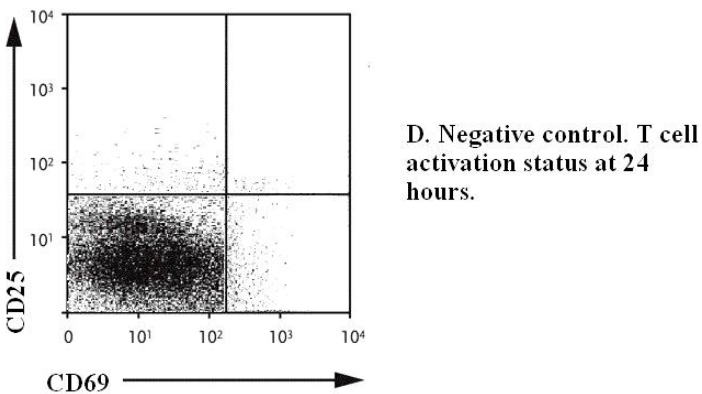B. Resting T lymphocytes
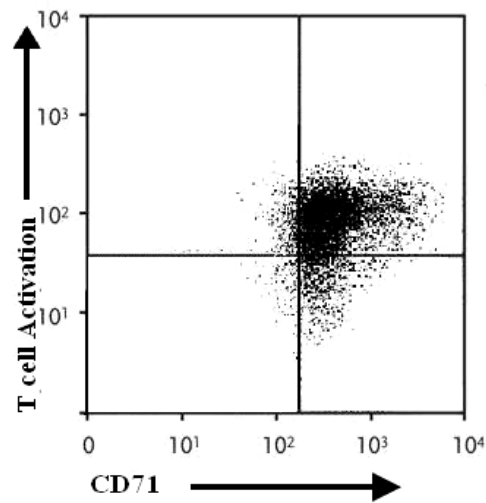
C. Alloreactive T lymphocytes

D. CD3/CD28-activated T lymphocytes

Independent verification of inactivation/activation status of T lymphocytes using Flow Cytometry

Appendix C (continued). Flow Cytometry Directed Verification of T –lymphocyte

Activation Status.

A. T cell activation at 24 hours.

B. T cell activation at 36 hours.

C. T cell activation at 48 hours.

D. T cell activation at 72 hours.

Mitogen activated T lymphocytes. As activation continues there is a dissapearence of nonactivated T cells and a decrease in CD69 positive T cells while the CD25 T cell population increases. [note: there are different cell concentrations at each FACS analysis with the least amount of cells being 2.4 x 10^6 (72 hours) and the most being 1 x 10^7 (24 hours)].

D. Negative control. T cell activation status at 24 hours.

Mitomycin C treated T lymphocyte. The population density of the T cells are concentrated in the lower left hand quadrant demonstrating that the expression of CD69 and CD25 is low. [note: there is not absolute restriction to this quadrant because the cross-hatched quadrants are somewhat arbitrary and is not linked to functional assay data]

Appendix D. Raw data images from cellular preparations

Overlay image of urine derived epithelial cells at 40x

Urine-derived T cells at 40x

Blood-derived T cells at 40x

T cell image at 50x on micro-Raman viewer

Image is example of T cells that were not selected for Raman analysis due to cell surface stipeling and "string of pearl" appearence of nuclei. Both are signs of apoptosis.

Image of CD3/CD28 Dynal activation bead (left) noting that the diameter is approximately the same as that of a T cell (~10-12 micrometers)

Appendix D (Cont.). Raw data images from cellular preparation

Immunomagnetic bead directed toward B lymphocytes were used to purify T lymphocyte

samples. Note the B lymphocytes (~10 micrometers) are attaching to the pro-B lymphocyte

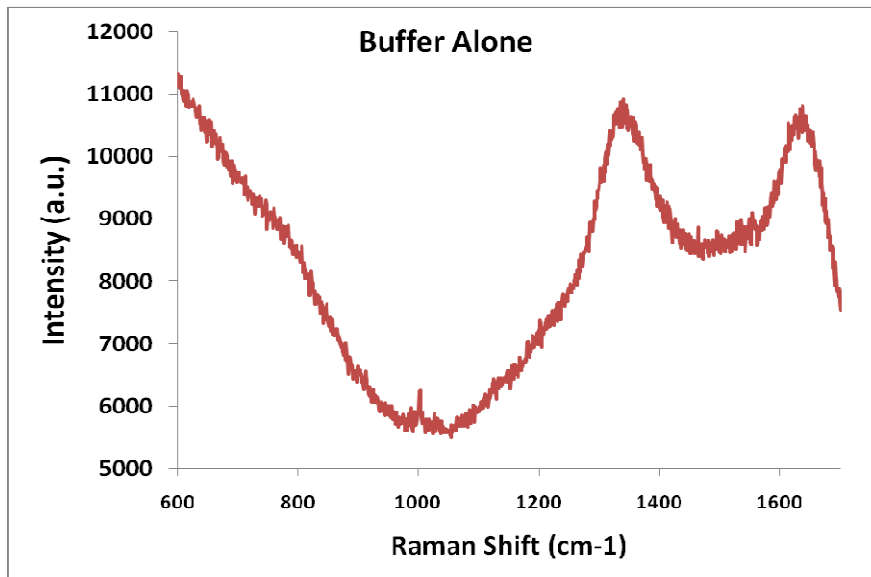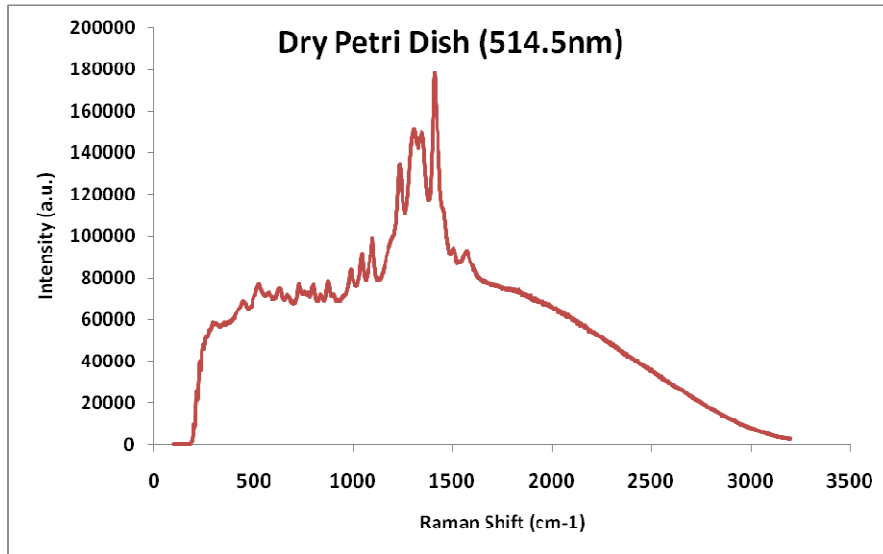antigens coating the bead which is several magnitudes larger.
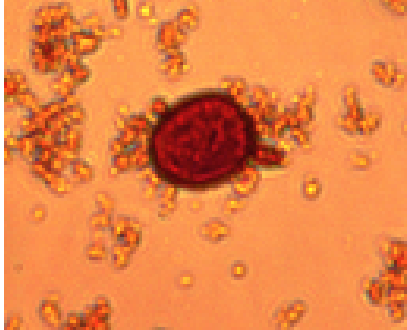
Appendix E. Reference and Control Raman Spectra

Appendix F. Human Investigation Committee Approval

WAYNE STATE UNIVERSITY

HUMAN INVESTIGATION COMMITTEE
101 East Alexandrine Building
Detroit, Michigan 48201
Phone: (313) 577-1628
FAX: (313) 993-7122
http://hic.wayne.edu

Full AAHRPP Accreditation

NOTICE OF EXPEDITED APPROVAL

To: Scott Gruber
Surgery
Harper University Hospital

From: James E. Puklin, M.D. _____
Chairman, Human Investigation Committee

Date: November 03, 2008

RE: HIC #: 097108M1E

Protocol Title: Raman Spectroscopic Detection of Acute Renal Allograft Rejection

Sponsor: Surgery

Protocol #: 0809006363

Expiration Date: November 02, 2009

Risk Level / Category: No greater than minimal risk.

The above-referenced Protocol and items listed below (if applicable) were **APPROVED** following *Expedited Review* (Category 23*) by the Chairperson/designee *for* the Wayne State University Institutional Review Board (M1) for the period of 11/03/2008 through 11/02/2009. This approval does not replace any departmental or other approvals that may be required.

- Receipt of signed HIPAA Summary Form, revised per HIC request of 09/24/08.
- Receipt of Informed Consent, dated 10/28/08, revised per HIC requests.
- Receipt of Research Protocol, revised per HIC request.
- Receipt of Data Collection Tool.

Federal regulations require that all research be reviewed at least annually. You may receive a *"Continuation Renewal Reminder"* approximately two months prior to the expiration date; however, it is the Principal Investigator's responsibility to obtain review and continued approval *before* the expiration date. Data collected during a period of lapsed approval is unapproved research and can *never* be reported or published as research data.

All changes or amendments to the above-referenced protocol require review and apprval by the HIC **BEFORE** implementation.

Adverse Reactions/Unexpected Events (AR/UE) must be submitted on the appropriate form within the timeframe specified in the HIC Policy (http://www.hic.wayne.edu/hicpol.html).

NOTE:

1. Upon notification of an impending regulatory site visit, hold notification, and/or external audit the HIC office must be contacted immediately.

2. Forms should be downloaded from the HIC website at *each* use.

*Based on the Expedited Review List, revised November 1998

Appendix G. List of Key Abbreviations

- APC- Antigen Presenting Cell

- AR- Acute Rejection

- CAN- Chronic Allograft Nephropathy

- CMV- Cytomegalovirus

- DFA- Discriminant Function Analysis

- ESRD- End Stage Renal Disease

- HIC- Human Investigation Committee

- HLA- DR- Human Leukocyte Antigen –DR

- Ig- Immunoglobulin

- mAb- Monoclonal Antibody

- MHC- Major Histocompatibility Complex

- MLC- Mixed Lymphocyte Culture (also referred to as Mixed Lymphocyte Reaction (MLR)

- RS- Raman Spectroscopy

- PCA- Principal Component Analysis

- PCR- Polymerase Chain Reaction

- SCAR- Subclinical Acute Rejection

REFERENCES

1. Bogman M and Dooper M. 1995. Banff classification for the histologic diagnosis of renal graft rejection: what are the advantages? Nephrol Dial Transplant, Editorial comments: p. 1291-1293.

2. Histology slides of acute rejection grades. [cited 2009 Nov 12]. Pathopic virtual histology image bank. Pathorama. http://alf3.urz.unibas.ch/pathopic/e/intro.htm.

3. Deng, H., Bloomfield, V.A., Benevides, J.M., Thomas, G.J. 1999. Dependence of the Raman signature of genomic B-DNA on nucleotide base sequence. Biopolymers. V50: p. 656 - 666.

4. Erfurth, S. C., Peticolas, W.L. 1975. Melting and premelting phenomenon in DNA by laser Raman scattering. Biopolymers. 14: p. 247–264.

5. Benevides, J. M., and G. J. Thomas. 1983. Characterization of DNA structures by Raman spectroscopy: high-salt and low-salt forms of double helical poly (dG-dC) in H2O and D2O solutions and application to B, Z and A-DNA. Nucleic Acids Res 11: p. 5747–5761.

6. Puppels, G. J., Demul, F., Otto, C., Greve, J., Robertnicoud, M., Arndtjovin, D.J., Jovin, T.M. 1990. Studying single living cells and chromosomes by confocal Raman microspectroscopy. Nature V347: p. 301–303.

ABSTRACT

RAMAN SPECTROSCOPIC MODELING OF T- LYMPHOCYTE ACTIVATION AND DETECTION OF ACUTE RENAL ALLOGRAFT REJECTION

by

KRISTIAN L. BROWN

May 2010

Advisor: Gregory Auner, PhD

Major: Biomedical Engineering

Degree: Doctor of Philosophy

Despite the advances made in the area of kidney transplantation, the disparity between the demand for and supply of available donated organs remains a dominant and unresolved issue. Given the paucity of available renal allografts, the preservation of existing grafts is vital. One factor that has negatively impacted renal allograft survival is acute rejection (AR). Traditionally, kidney transplant centers have used elevations in serum creatinine as a screening tool for detecting AR. However, with its diagnostic delay, low sensitivity, and low specificity, serum creatinine has proven to be an unreliable and problematic bio-marker. AR is an activated T lymphocyte driven process that leads to graft dysfunction and possible loss. The activation state of T lymphocytes is determined by the specific cell surface receptor composition present. A technologic tool that could resolve these receptor differences could detect T lymphocyte activation and thus provide a diagnostic modality for AR. Raman spectroscopy (RS), a laser-based technology that is able to characterize substances based on molecular vibrational signatures, represents this modality. Using T lymphocytes isolated from human peripheral blood and clean-catch urine we investigated three aspects of T lymphocyte activation using a modified RS system. First, we explored the *sensitivity* (the ability to detect activation) of a RS-based system by analyzing mixed lymphocyte reacted (MLR), mitomycin C inactivated, and resting T

lymphocytes at 785nm and 514.5nm wavelengths. Second, the *specificity* (the ability to distinguish T cells activated by different stimuli) of the system was determined by comparing the signatures of MLR and CD3/CD28-activated T lymphocytes. Third, we analyzed the biomolecular events that conveyed the spectral changes detected by RS. This was carried out by coupling RS analysis of Mitogen-activated T lymphocytes with antigen expression kinetic studies designed to quantify the intensity and timing of cell surface receptor up-regulation. We found that there were significant RS signature differences between the MLR and non-activated (inactivated and resting) T lymphocytes while there was only a trend toward differences seen between the resting and inactivated cellular populations. When analyzing MLR versus CD3/CD28-activated cells, both samples differed from the inactivated and resting groups and demonstrated differences in Raman shifts at multiple foci when compared with one another. Receptor expression kinetics of mitogen-activated T lymphocytes analyzed at the early and late phases of activation showed differential antibody immuno-fluorescent intensity. This correlated with spectral differences at defined peaks. Moreover, when analyzing all forms of activation (i.e. MLR, CD3/CD28, or mitogen) there were conserved and reproducible signature changes regardless of mode of activation which supports the notion that there are receptor and receptor moiety changes that are required in all forms of T lymphocyte activation. This dissertation outlines the use of RS in the resolution and modeling of cell surface receptor differences that define T lymphocyte activation. The accurate detection of T lymphocyte activation within a biomatrix is the foundational step toward the development of a noninvasive tool capable of accurately detecting AR in real-time within the clinical setting.

AUTOBIOGRAPHICAL STATEMENT

EDUCATION AND TRAINING

Surgical Residency	Department of General Surgery, Wayne State University School of Medicine (present)
Post Graduate Education (PhD)	Doctoral Candidate Biomedical Engineering, Wayne State University, Department of Bioengineering, College of Engineering: Drs. Scott Gruber and Gregory Auner (present)
Graduate Education (MD)	Doctorate of Medicine, University of California, San Diego School of Medicine (2005)
Undergraduate Education (BS)	Bachelors of Science- Cell and Molecular Biology, San Diego State University (2001)
RESEARCH INTERESTS	Noninvasive detection of acute kidney rejection, Tissue engineered functional nephrons from induced pleuripotent cells

SELECTED PUBLICATIONS

- Gruber SA, **Brown KL**, El-Amm JM, Singh A, Mehta K, Morawski K, Cincotta E, Nehlsen-Cannarella S, Losanoff JE, West MS, Doshi, MD. Equivalent outcomes with primary and retransplantation in African-American deceased-donor renal allograft recipients. *Surgery.* Sept 2009;146(4):646-52; discussion 652-3.

- **Brown KL**, Palyvoda OY, Thakur JS, Nehlsen-Cannarella SL, Fagoaga OR, Gruber SA, Auner GW. Differentiation of Alloreactive versus CD3/CD28 stimulated T- lymphocytes Using Raman Spectroscopy: A greater specificity for noninvasive acute renal allograft rejection detection. *Cytometry A*. 75: 917-23, 2009.

- **Brown KL**, El-Amm JM, Doshi MD, Singh A, Cincotta E, Morawski K, Losanoff JE, West MS, Gruber SA. Outcome predictors in African-American deceased-donor renal allograft recipients. *Clin Transplant*. 2009 Aug;23(4):454-61.

- **Brown KL**, Palyvoda OY, Thakur JS, Nehlsen-Cannarella SL, Fagoaga OR, Gruber SA, Auner GW. Raman spectroscopic differentiation of activated versus non-activated T lymphocytes: an in vitro study of an acute allograft rejection model. *J Immunol Methods*. 2009 Jan 1;340(1):48-54.

- Gruber SA, Doshi MD, Cincotta E, **Brown KL**, Singh A, Morawski K, Alangaden G, Chandrasekar P, Losanoff JE, West MS, El-Amm JM. Preliminary experience with renal transplantation in HIV+ recipients: low acute rejection and infection rates. *Transplantation*. 2008 Jul;86(2):269-74.

- **Brown KL**, El-Amm JM, Doshi MD, Singh A, Morawski K, Cincotta E, Siddiqui F, Losanoff JE, West MS, Gruber SA. Intermediate-term outcomes of hepatitis C-positive compared with hepatitis C-negative deceased-donor renal allograft recipients. *Am J Surg*. 2008 Mar;195(3):298-302; discussion 302-3.